Review

Inferring Neurocognition and Intelligence using Brain MRI

Mohammad Arafat Hussain , Ellen Grant , Yangming Ou *

Posted Date: 3 March 2023

doi: 10.20944/preprints202302.0452.v2

Keywords: Neurocognition; MRI; Intelligence; Brain

Review

Inferring Neurocognition and Intelligence Using Brain MRI

Mohammad Arafat Hussain, P. Ellen Grant and Yangming Ou *

Department of Pediatrics; Radiology; Boston Children's Hospital, Harvard Medical School, 401 Park Drive, Boston, MA 02115, USA

* Correspondence: Yangming.Ou@childrens.haravard.edu

Abstract. Brain magnetic resonance imaging (MRI) offers a unique lens to study neuroanatomic support of human neurocognition and intelligence. A core mystery is the MRI explanation of individual differences in neurocognition and intelligence. The past four decades have seen great advancement in studying this century-long mystery, but the sample size and population-level studies limit the explanation at the individual level. The recent rise of big data and artificial intelligence offers novel opportunities. Yet, data sources, harmonization, study design, and interpretation need to be carefully considered. This review aims to summarize past work, discuss rising opportunities and challenges, and facilitate further investigations on machine intelligence inferring human intelligence.

Keywords: neurocognition; MRI; intelligence; brain

Introduction

Neurocognition refers to the *mental process* of learning, solving problems, remembering, and appropriately using information from memory.[1] On the other hand, intelligence refers to different *mental abilities* such as problem-solving, logic, reasoning, and planning. Intelligence describes *neurocognition quality* in people.[2–4] A person's neurocognition and intelligence are important factors in this person's education, career, social status, health, and longevity.[5] Yet, how can we explain the substantial differences among people in their neurocognition and intelligence? Can we effectively measure a person's neurocognition and intelligence? Can we predict a person's future course of neurocognition and intelligence, in normal and disease? Seeking answers to these questions is at the core of neuroscience research for over a century. The hope is to identify and boost each individual's potential (different people are "smart" in different ways),[6] and to early intervene and improve outcomes for those vulnerable.[7,8]

Besides genetic factors,[9] differences in neuroanatomy and brain connectivity are widely believed to contribute to individual variability of neurocognition and intelligence.[6] Early studies (the 1900s) related neurocognitive functions to brain structures in post-mortem brains.[10] The invention of magnetic resonance imaging (MRI) in 1977 has allowed for in vivo three-dimensional (3D) study of brain structure and function. Advancement in MRI analytics in the past 4 decades further brings the automated, quantitative, and sophisticated investigation of neuroanatomy[11,12], white matter integrity[13,14], and brain circuit connectivity[15], which are all found correlated to neurocognitive and intelligence test scores.[6,11] Sample sizes, however, were often dozens to lower hundreds; findings were not always consistent; and population-level associations have not yet been reliably translated into individual prediction.

With very recent availability in big data brain MRI (over 1,000 or even 10,000 individuals),[16] coupled with the rise of artificial intelligence (AI),[17] offers promises to revolutionize MRI inference of neurocognition and intelligence. While opportunities arise, open issues on the data source, merging, harmonization, analytics, target test scores, study design, and interpretations need to be considered. While there is a recent review,[18] which mostly focused on discussing existing MRI studies that correlate brain biology to human intelligence, this review comprehensively discusses existing MRI studies focusing on human neurocognition and intelligence predictive tasks, open issues, and rising

Preprints (www.preprints.org) | NOT PEER-REVIEWED | Posted: 3 March 2023 doi:10.20944/preprints202302.0452.v2

opportunities. The aim is to facilitate further studies of machine intelligence inferring human intelligence.

Measurement of Human Intelligence and Neurocognition

Assessment of intelligence is often approximated by the assessment of neurocognitive abilities.[2–4] Intelligence is positively correlated to the processing speed,[4] executive functions,[19,20] general memory,[21] and working memory,[22] as these neurocognitive abilities are assessed as broad abilities in a typical intelligence assessment system (see Box 1).

Box 1. Measuring intelligence and neurocognition based on the CHC theory.

Cattell–Horn–Carroll's (CHC) Theory for Human Intelligence: The CHC theory[23] is widely accepted as a backbone for many of today's tests for human intelligence and neurocognition. The CHC theory divides human intelligence into three stratums[24], as first laid out by Carroll in 1993 and later enriched by Cattel and Horn,[25], and other researchers. As Fig 1 shows, the very top stratum in the CHC theory is a general intelligence (g),[26] named by Spearman[26] in 1904. The general intelligence g is a fundamental ability that supports all domains of neurocognitive abilities.[26] It can be further divided into "broad abilities" (middle stratum). These broad abilities first include general fluid (gF) and crystallized (gC) intelligence factors, the so-called gF-gC model as proposed by Cattell et al in 1963.[27] gF refers to the ability of reasoning and solving new problems while gC refers to the knowledge and experience accumulated over time. The broad abilities in the middle stratum also include short-term memory and learning ability (gY), long-term retrieval ability (gR), visual perception (gV), auditory perception (gU), cognitive speediness (gS), and processing speed (gT). Each of these broad abilities is subdivided into narrow abilities (the bottom stratum in Figure 1). The original 1993 version of the CHC theory has several variations in the 2010s[28] and its history has been detailed online.[29]

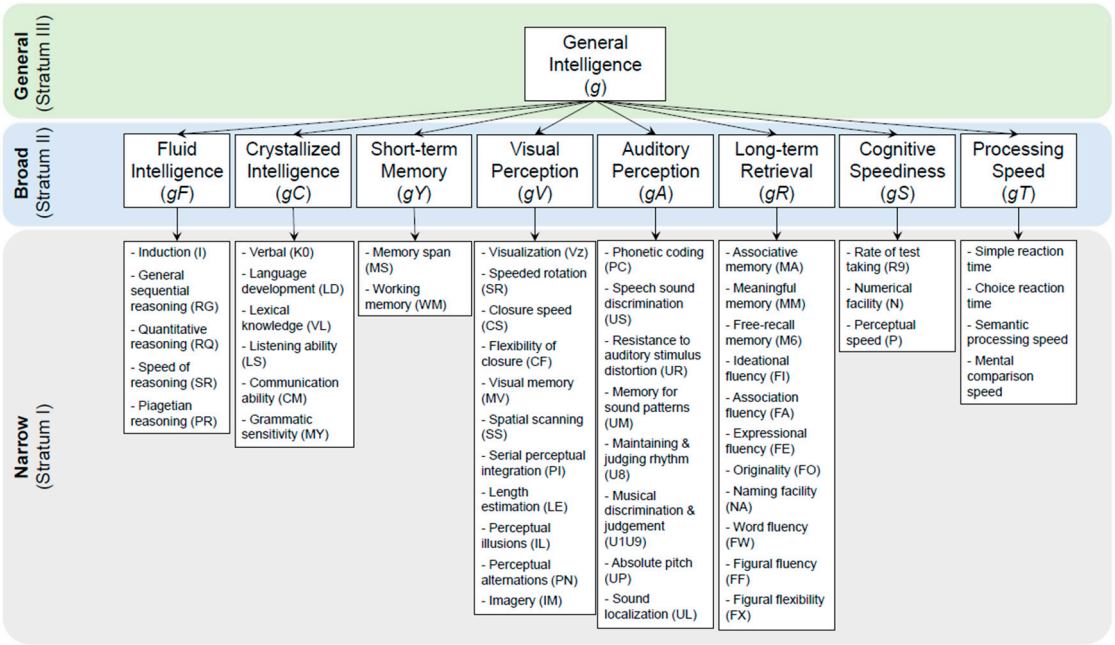

Figure 1. The Cattell-Horn-Carrol (CHC) Theory divides the general intelligence g (top stratum), which is hard to measure, into 8-10 broad abilities (middle stratum) and over 60 narrow abilities (bottom stratum), which are more measurable. Measuring these narrow abilities is the core of many of today's neurocognitive and intelligence tests.

Preprints (www.preprints.org) | NOT PEER-REVIEWED | Posted: 3 March 2023 doi:10.20944/preprints202302.0452.v2

Intelligence and Neurocognition Tests: The CHC theory turns the difficult task of measuring the general intelligence *g* into more feasible tests of measuring 8-10 broad abilities and over 60 narrow abilities (middle and bottom stratum). Many of today's intelligence and neurocognitive tests are designed to score these narrow abilities (bottom stratum in the CHC theory).[23,30] Wechsler Adult Intelligence Scale IV (WAIS-IV)[31], for example, assesses five different broad abilities (*gC*, *gS*, *gV*, *gF*, and *gY*) to estimate the full-scale intelligence quotient (FSIQ) as a proxy of *g*. Specifically, WAIS-IV tests the narrow abilities such as vocabulary, comprehension, similarities, information, and arithmetic, to assess the broad ability *gC*; other narrow abilities such as symbol search, coding, and cancellation to assess the broad ability *gS*; narrow abilities such as visual puzzles, block design, and picture completion to assess the broad ability *gV*; narrow abilities figure weights, arithmetic matrix, and reasoning to assess the broad ability *gF*; and other narrow abilities such as digit span, and letter-number sequencing to assess the broad ability *gY*.[32] Similar sub-factoring for IQ scoring is also used for other popular scoring systems such as Wechsler Intelligence Scale for Children-V (WISC-V),[33] Wechsler Abbreviated Scale of Intelligence-II (WASI-II),[34] Woodcock-Johnson Tests of Cognitive Abilities-III (WJ-III)[35], Mullen Scales of Early Learning (MSEL),[36] and Bayley Scales of Infant Development (BSID)[37], and others.

Cognitive Test Batteries: Although FSIQ is a good indicator of overall cognitive ability, it is also a composite score of different broad abilities. Thus, the FSIQ score often does not express the extent of cognitive impairment in single domains. Further, a deficit in one subtest (i.e., a deficit in one broad ability) is often compensated by a better performance in another subtest during FSIQ scoring.[38] Hence, to examine a specific broad ability, different cognitive test batteries are widely used. Like conventional IQ tests, cognitive test batteries score human cognitive performance in several domains using subtests. Many domains overlap with the CHC's broad abilities, however, they also include additional domains like executive function and language performance.[39] For example, the neuropsychological assessment battery (NAB)[40] assesses five cognitive domains such as attention, language, memory, spatial, and executive functions. Another popular and widely used test battery, the NIH toolbox of neurocognitive battery (NIH-TCB)[41] is designed to measure executive function, attention, episodic memory, language, processing speed, and working memory (see Figure 2).[42]

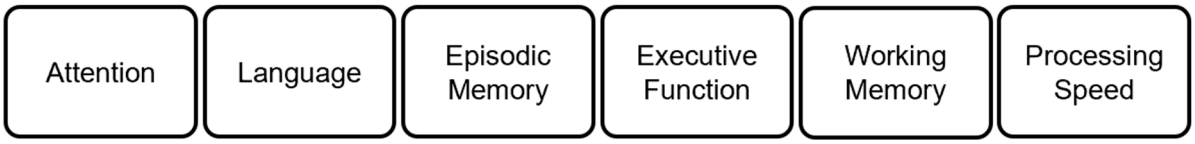

Figure 2. Domains scored by the NIH toolbox neurocognitive battery.

Theories linking brain structure and neurocognitive function

Neuroimaging studies since the 1980s have given rise to theories about brain structure-function mapping. Examples include network neuroscience theory (NNT),[43] lateral prefrontal cortex theory (LPFCT),[44] multiple-demand theory (M-DT),[45] and process overlap theory (POT).[46] Among these popular theories is the Parieto-Frontal Integration Theory (P-FIT), proposed by Jung and Haier in 2007, after reviewing 37 structure-function neuroimaging studies.[47] The P-FIT theory, as detailed in Box 2, is influential as it offers insights that human intelligence/ neurocognition resides in large-scale connected brain regions known as brain networks.[48]

Preprints (www.preprints.org) | NOT PEER-REVIEWED | Posted: 3 March 2023 doi:10.20944/preprints202302.0452.v2

Box 2. The P-FIT Theory for Distributed Brain Network underlying Human Intelligence.

The P-FIT theory emphasizes network integrity most in the sustenance of human intelligence.[18] The P-FIT theory involves four information processing stages, each involving different Brodmann areas (BAs) in the connected brain networks[47,49] (see Figure 3):

Stage 1. It is assumed that humans *first* gather and process sensory information predominantly in the occipital and temporal areas. Early processing of sensory information happens in the extrastriate cortex (BAs 18 and 19). Recognition, imagery, and elaboration happen in the fusiform gyrus (BA 37). Analysis and elaboration of auditory information syntax happen in Wernicke's area (BA 22).

Stage 2. This stage involves the structural symbolism, abstraction, and elaboration of the basic sensory information (in Stage 1) in the angular gyrus (BA 39), supramarginal gyrus (BA 40), and superior parietal lobule (BA 7).

Stage 3. This stage involves the interaction between parietal areas and frontal lobes (BAs 6, 9,10, 45, 46, and 47). This interaction supports problem-solving, evaluation, and hypothesis testing.

Stage 4. Once the best solution is reached, the anterior cingulate (BA 32) gets engaged for response selection and inhibition of competing responses.

The P-FIT theory emphasizes that the whole process (Stages 1-4) depends upon the fidelity of underlying white matter connectivity. White matter facilitates rapid and error-free data transmission from the posterior to frontal brain regions. Note that the P-FIT model considers only those Brodmann areas, which appeared in more than 25% of the total 37 studies Jung and Haier[47] reviewed. Table 1 covers a full spectrum of Brodmann areas that Jung and Haier have summarized[47].

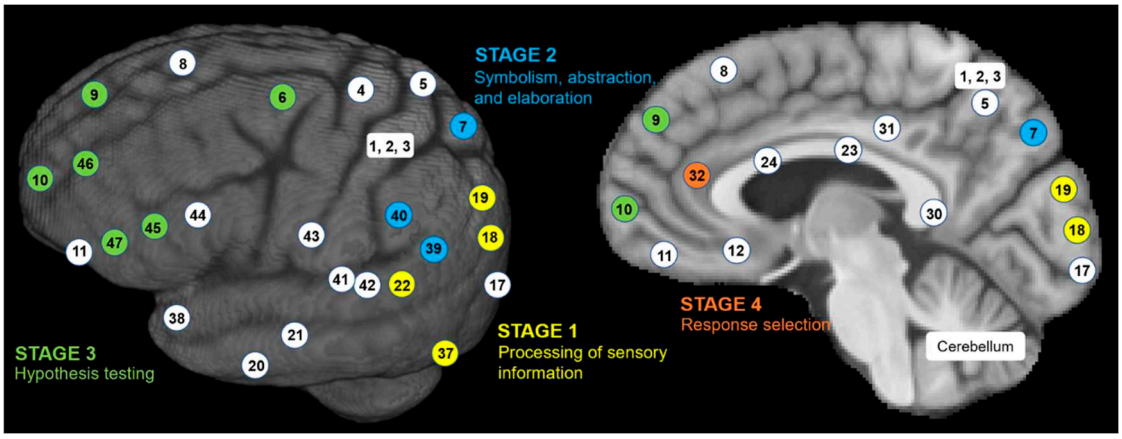

Figure 3. Sensory information processing stages by the P-FIT model. Brodmann area (BA) numbers are color coded to correspond to different stages of information processing.

Preprints (www.preprints.org) | NOT PEER-REVIEWED | Posted: 3 March 2023 doi:10.20944/preprints202302.0452.v2

Table 1. Brodmann areas were found to be related to human cognition and intelligence in a total of 37 studies over 1,557 subjects, reported by Jung and Haier in 2007[47]. Only shaded columns of Bas comprise the P-FIT model. Acronyms- BA: Brodmann Area, LH: Left Hemisphere, RH: Right Hemisphere.

	Frontal Lobe													Cingulate Cortex						Parietal Lobe					Insula	Temporal Lobe							Occipital Lobe			
BA Name	Primary motor cortex	Premotor & Suppl. Motor	Frontal eye field	Dorsolateral prefrontal cortex	Anterior prefrontal cortex	Orbital and rectus gyri	Orbitofrontal area	Insular cortex	Pars opercularis	Pars opercularis	Dorsolateral prefrontal cortex	Pars orbitalis	Parasubicular area	Ventral posterior cingulate	Ventral anterior cingulate	Part of cingulate cortex	Dorsal Posterior cingulate	Dorsal anterior cingulate	Primary Somatosensory Cortex	Somatosensory Assoc. Cortex	Somatosensory Assoc. Cortex	Angular gyrus	Supramarginal gyrus	Primary gustatory cortex	Insular cortex	Inferior temporal gyrus	Middle temporal gyrus	Superior temporal gyrus	Fusiform gyrus	Temporopolar area	Auditory cortex	Auditory cortex	Primary visual cortex (V1)	Secondary visual cortex (V2)	Associative visual cortex (V3-)	Cerebellum
BA #	4	6	8	9	10	11	12	13	44	45	46	47	49	23	24	30	31	32	3	5	7	39	40	43	13	20	21	22	37	38	41	42	17	18	19	
LH		X	X	X	X	X	X	X	X	X	X	X		X	X	X	X	X		X	X	X	X			X	X	X	X	X	X	X	X	X	X	X
RH	X	X	X	X	X	X	X		X	X	X	X	X		X	X	X	X	X	X	X	X	X	X	X	X	X	X	X	X			X	X	X	X

Structural MRI to Infer Intelligence and Neurocognition

Typical brain MRIs include structural, diffusion, functional, and other sequences. This section starts with structural MRI (sMRI) and its inference of human intelligence and neurocognition. sMRI includes T1-, T2-weighted MRI (T1/T2-MRI), proton density, and other sequences. Subsections below will introduce morphometric features from sMRI (see review for more details[50]) and their use of them to infer neurocognition and intelligence.

Regional Brain Volume to Infer Neurocognition/Intelligence. Software packages such as FreeSurfer,[51] FSL,[52] AFNI,[53] and others (see review[54]) allow us to automatically segment the T1- or T2-weighted brain MRIs into hemispheres (left and right), tissue types (white matter, gray matter, cerebrospinal fluid), and regions using single/multi-atlas[55] or machine learning[56] approaches. The volumes of these structures have been used to correlate with neurocognition or intelligence test scores.

Early studies argued that the attentional control mechanism, the linkage between sensory discrimination and intelligence,[57] corresponds to the volumes in brain regions such as lateral fronto-parietal cortex[58] (includes BAs 6, 8, 9), dorsal anterior cingulate[58,59] (includes BA 32), and lateral posterior cerebellum.[58] As summarized in Table 3 of the supplementary materials, recent structural MRI-based predictive methods[55,60–70] that used brain regional volumes found that the fronto-parietal (includes BAs 6, 8, and 9), cingulo opercular (includes BAs 22, 41, and 42), visual (includes BAs 17, 18, and 19), somatosensory (includes BAs 1, 2, 3, 5, and 7), right posterior cingulate gyrus (BAs 23, 31), left caudate nucleus, entorhinal white matter (BA 28), globus pallidus, precentral gyrus (BA 4), corpus callosum, left/right hippocampus, parahippocampal gyrus (BA 34), thalamus, precentral gyrus (BA 4), caudate nucleus, pons, and motor (includes BAs 4 and 6) cortex areas are related to the fluid intelligence in adolescents. This study predicted the residual fluid intelligence score of more than 3500 adolescents with a mean square error (MSE) ranging from 92 to 101 (for a range of true residual fluid intelligence score of [-40, 30]),[55,60–69] or a correlation of 10% ($p < 0.05$),[70] which further strengthens the arguments from the previous studies[58,71,72] as well as the P-FIT theory. Another study[73] involving a comparatively smaller adult data cohort (N = 211) reported a positive correlation of overall gray matter volume with fluid intelligence ($r = 0.16$; $p < 0.01$), working memory ($r = 0.21$; $p < 0.01$), and quantitative reasoning ($r = 0.26$; $p < 0.01$). Similar findings are reported for an infant data

 doi:10.20944/preprints202302.0452.v2

cohort,[74] where the pre-term fetal growth restricted (P-FGR) infants group had lower mean gray matter, white matter, thalamic, cerebellar white matter, and hippocampal volumes compared to that of pre-term appropriate gestational age (PT-AGA) and term AGA (T-AGA). This difference in brain volumes is reflected in the mean FSIQ scores of PT-FGR and PT-AGA groups, 80 and 103, respectively.[74] Insight test battery (ITB)-based cognitive scores can also be predicted ($p < 0.001$) from gray matter volumes in the right insula, right middle cingulate cortex/precuneus (BAs 13, 14, 16, 4).[75] Another study[76] used relative gray matter volume per voxels from the region of fronto-parietal network (includes BAs 6, 8, and 9), default mode network (includes BAs 38, 25, 23, 31, and 4), dorsal attention network (includes BAs 17, 18, 19, 8, 7, and 6), and cerebellum in principal component analysis (PCA) and showed an MSE and correlation between the actual and estimated FSIQ is 320 ($p = 0.279$) and $r = 0.11$, respectively (for true residual FSIQ in the range of [39, 136]). The caudate also plays a vital role in the rewarding system of human reinforcement learning during making a choice and action,[77,78] and a significant positive correlation ($r = 0.24$; $p = 0.01$) between the caudate volume and FSIQ is also reported.[79]

Cortical Surface Metrics to Infer Neurocognition/Intelligence. In addition to the regional brain volumes, metrices on cortical surface also play a vital role in inferring human intelligence. Automated software such as FreeSurfer can reconstruct brain cortical surfaces, and extract cortical surface areas, cortical thickness, cortical folding curvatures, and gyrification indices. Previous studies reported that information integration and processing happen in the parahippocampal gyrus (includes BA 34) and precuneus/cuneus cortex[11,80] (includes BAs 4, 19), visual identification and recognition happen in the ventral temporal cortex[81,82] and integration and retrieval of semantic knowledge happen in the medial temporal lobes[83] (includes BA 38).

Table 3. Summary of sMRI studies correlating regional brain volumes with neurocognition/intelligence. Acronyms- ANCOVA: Analysis of Covariance, ABCD: Adolescent Brain Cognitive Development, NKI: Nathan S. Kline Institute for Psychiatric Research, NIH-TCB: NIH toolbox of neurocognitive battery, PCA: Principal Component Analysis, LASSO: Least Absolute Shrinkage and Selection Operator, SVM: Support Vector Machine, SVR: Support Vector Regression, RF: Random Forest, LR: linear regression, RR: ridge regression, MLP: multi-layer perceptron, CNN: Convolutional Neural Network, ROI: Region of Interest, KNN: K-Nearest Neighbors, MSE: Mean Square Error, RMSE: Root MSE, WASI: Weschler Abbreviated Scale of Intelligence, WISC: Wechsler Intelligence Scale for Children, WAIS: Wechsler Adult Intelligence Scale, FSIQ: Full-scale Intelligent Quotient, BOMAT: Bochum Matrices Test, T1-w: T1-weighted MRI, T2-w: T2-weighted MRI, P-FGR: Pre-term Fetal Growth Restricted, PT-AGA: Pre-term Appropriate Gestational Age, T-AGA: Term AGA, DTI: Diffusion Tensor Imaging, ICV: intracranial volume, WM: white matter, GM: gray matter, CSF: cerebrospinal fluid, N/A: not available, not mentioned. Probable BAs are not specified for either left or right hemisphere.

Study	Year	N	Age (years)	Dataset	MRI type	MRI features	Regions	Probable BAs	IQ/ Neuro. Test	Normal/ Abnormal	Method	Correlation/ Finding
Saha et al.[70]	2021	7709	9-10	ABCD	T1-w	CNN learned features and volumes of manually identified brain regions	GM regions of left/right hippocampus, parahippocampal gyrus, thalamus, precentral gyrus and caudate nucleus; WM region of the pons.	34, 4	NIH-TCB	Normal	CNN and MLP	Correlation between the actual and predicted *gF* = 0.1 ($p < 0.05$)
Hilger et al.[76]	2020	380	18-60	NKI-Rockland-Enhanced	T1-w	GM volume per voxel	Frontoparietal network, default mode network, Dorsal attention network, and cerebellum	38, 25, 23, 31, 4, 17, 18, 19, 8, 7, 6, 9	WASI	Normal	PCA	MSE and correlation between the actual and estimated FSIQ is 320 ($p = 0.279$) and 0.11, respectively (for true residual FSIQ in the range of [39, 136])
Chiang et al.[60]	2019	8669	9-10	ABCD	T1-w	Total volume, mean signal intensity, and entropy	Visual, frontoparietal, somatosensory, motor, default mode	6, 8, 9, 22, 41, 42, 17, 18, 19, 1,	NIH-TCB	Normal	CNN, and LASSO	Mean Square Error *(gF)* = 95.38 (for true residual *gF* in

doi:10.20944/preprints202302.0452.v2

							network, and cingulo opercular network.	2, 3, 5, 7, 4				the range of [-40, 30])
Shrivastava et al.[61]	2019	8669	9-10	ABCD	T1-w	Volume, mean intensity, and count of GM voxels	Gyrus rectus, hippocampus, inferior frontal gyrus, middle frontal gyrus, postcentral gyrus, precentral gyrus, precuneus, superior frontal gyrus and supramarginal gyrus.	11, 44, 45, 47, 4, 1, 2, 3, 10, 12, 40	NIH-TCB	Normal	CNN, SVR, RF, gradient boosting, and XGBoost	Mean Square Error *(gF)* = 93.68 (for true residual *gF* in the range of [-40, 30])
Ren et al.[62]	2019	8669	9-10	ABCD	T1-w	ROI volumes	GM	11, 44, 45, 47, 4, 1, 2, 3, 10, 12, 40	NIH-TCB	Normal	Bagging and boosting of LR, RR, RF, envelope-based reduced-rank regression, LASSO, Elastic-Net regressor, and KNN	Mean Square Error *(gF)* = 92.99 (for true residual *gF* in the range of [-40, 30])
Tamez-Pena et al.[63]	2019	8669	9-10	ABCD	T1-w	ROI volumes	GM, WM, CSF, and cerebellum	11, 44, 45, 47, 4, 1, 2, 3, 10, 12, 40	NIH-TCB	Normal	Ensemble of SVM, RF, and bootstrapped step wise model selection	Mean Square Error *(gF)* = 100.89 (for true residual *gF* in the range of [-40, 30])
Brueggeman et al.[64]	2019	8669	9-10	ABCD	T1-w	122 ROI volumes	GM, WM, CSF	11, 44, 45, 47, 4, 1, 2, 3, 10, 12, 40	NIH-TCB	Normal	RF	Mean Square Error *(gF)* = 92.49 (for true residual *gF* in the range of [-40, 30])

doi:10.20944/preprints202302.0452.v2

Mihalik et al.[65]	2019	8669	9-10	ABCD	T1-w	Voxel intensities and probabilistic tissue-type labels	GM, WM	11, 44, 45, 47, 4, 1, 2, 3, 10, 12, 40	NIH-TCB	Normal	Kernel ridge regressor	Mean Square Error *(gF)* = 92.13 (for true residual *gF* in the range of [-40, 30])
Ranjbar et al.[66]	2019	8669	9-10	ABCD	T1-w	122 ROI volumes	GM, WM, CSF	11, 44, 45, 47, 4, 1, 2, 3, 10, 12, 40	NIH-TCB	Normal	CNN and RF	Mean Square Error *(gF)* = 93.64 (for true residual *gF* in the range of [-40, 30])
Wlaszczyk et al.[67]	2019	8669	9-10	ABCD	T1-w	ROI volumes, signal intensity, anterior and posterior cross-sectional area from corpus callosum	GM and corpus callosum	11, 44, 45, 47, 4, 1, 2, 3, 10, 12, 40	NIH-TCB	Normal	RF	Mean Square Error *(gF)* = 92.93 (for true residual *gF* in the range of [-40, 30])
Zhang-James et al.[55]	2019	8669	9-10	ABCD	T1-w	122 ROI volumes	GM, WM, CSF	11, 44, 45, 47, 4, 1, 2, 3, 10, 12, 40	NIH-TCB	Normal	Nu SVM	Mean Square Error *(gF)* = 95.63 (for true residual *gF* in the range of [-40, 30])
Kao et al.[68]	2019	8669	9-10	ABCD	T1-w	122 ROI volumes	GM, WM, CSF	11, 44, 45, 47, 4, 1, 2, 3, 10, 12, 40	NIH-TCB	Normal	StackNet consisting of random forest, random tree, ridge regressor, and gradient boosting	Mean Square Error *(gF)* = 94.25 (for true residual *gF* in the range of [-40, 30])
Li et al.[69]	2019	8669	9-10	ABCD	T1-w	ROI volumes, # detected surface holes, the globus	Right posterior cingulate gyrus, left caudate nucleus, entorhinal white	23, 31, 28, 4, 1, 2, 3, 22	NIH-TCB	Normal	BlockPC-XGBoost	Mean Square Error *(gF)* = 93.16 (for true residual *gF* in

doi:10.20944/preprints202302.0452.v2

						pallidus volume, the mean curvatures of precentral gyrus, postcentral gyrus, and banks of Superior Temporal Sulcus	matter, globus pallidus, precentral gyrus, postcentral gyrus, and superior temporal sulcus					the range of [-40, 30])
Morsing et al.[74]	2018	74	7-8	Skane University Hospital in Lund, Sweden	T1-w	ROI volumes	ICV, GM, WM, CSF, and thalamus.	N/A	WISC-III	P-FGR, PT-AGA, and T-AGA	Chi-square and ANOVA	The mean (SD) FSIQ was 80 (17) in the PT-FGR group and 103 (12) in the PT-AGA group
Ogawa et al.[75]	2018	232	21-69	Advanced Telecommunication Research Institute International, Kyoto	T1-w	GM volume	Right insula, right middle cingulate cortex/precuneus	13, 14, 16, 4	Insight test battery (ITB)	Normal	Pearson correlation	ITB score was positively correlated with the GM volumes in the mentioned region ($p < 0.001$)
Paul et al.[73]	2016	211	18-44	University of Illinois Urbana-Champaign	T2-w	Volume fractions across tissue types	GM, WM, CSF	23, 31	BOMAT, Number Series, and Letter Set	Normal	Bivariate correlation	GM volume is found positively correlated with quantitative reasoning ($r = 0.26$; $p < 0.01$) and working memory ($r = 0.21$; $p < 0.01$),

doi:10.20944/preprints202302.0452.v2

												and *gF* (r = 0.16; p < 0.01)
Grazioplene et al.[79]	2015	517	18-40	University of Minnesota, University of New Mexico in Albuquerque, Yale University	T1-w MPRAGE	Caudate volume	Caudate nucleus	N/A	WAIS-III, WAIS-IV, WASI	Normal	LR	Regression of IQ onto bilateral caudate volume indicated a significant positive correlation between caudate volume and FSIQ (r = 0.24; p = 0.01)

doi:10.20944/preprints202302.0452.v2

 doi:10.20944/preprints202302.0452.v2

Cortical metrics are often combined with regional volumes to predict neurocognition. Studies using the ABCD dataset predicted the residual fluid intelligence score of more than 4500 adolescents with an MSE ranging from 93 to 95 (for a range of true residual fluid intelligence score of [-40, 30]), as summarized in Table 4 of the supplementary materials. These studies used cortical thicknesses, curvatures, and surface areas in conjugation with the regional volumes from the left middle temporal gyrus (BA 21), the right superior temporal gyrus (BA 22), left/right parahippocampal gyrus (BA 34), pons white matter, hippocampus, posterior cingulate gyrus (BAs 23, 31), cuneus (BA 19), left lingual gyrus (BA 19), left middle frontal gyrus (BA 10), supramarginal gyrus (BA 40), right fusiform gyrus (BA 37), superior temporal gyrus (BA 22), right anterior cingulate gyrus (BAs 24, 32, 33), and other brain structures.[84–89]

Significant positive correlations were also observed between the Reynolds intellectual assessment scales (RIAS) composite IQ scores and cortical gray matter volumes in the orbitofrontal gyrus (BAs 11, 12) ($r = 0.41$; $p = 0.03$), transverse temporal gyri (BAs 41, 42) ($r = 0.42$; $p = 0.02$), left superior temporal gyrus (BA 22) ($r = 0.41$; $p = 0.04$), and right anterior cingulate gyrus (BAs 24, 32, 33) ($r = 0.42$; $p = 0.03$).[90] The local gyrification and surface area in the superior parietal (BA 7), left supramarginal (BA 40), left caudal middle frontal (BA 22), left pars-opercularis (BA 44), left inferior temporal (BA 20), right inferior and middle temporal (BA 21), right medial orbitofrontal (BAs 11, 12), and right rostral middle frontal (BA 10) regions are also found correlated to gF ($r = 0.29$; $p < 0.001$) and ($r = 0.22$; $p < 0.001$), respectively, and to gC ($r = 0.28$; $p < 0.001$) and ($r = 0.28$; $p < 0.001$), respectively, on a healthy young dataset (age = 21-35 years).[91] In another study,[92] significant positive relationship between cortical thickness in the superior parietal lobe (BA 7) and FSIQ, PIQ, and VIQ is seen at a cluster-forming threshold (CFT) of $p < 0.05$. Similarly, positive relationship between cortical volume in the inferior parietal lobe (BAs 39, 40) and FSIQ and PIQ is seen at a CFT of $p < 0.05$. Additionally, cortical volume is found positively associated with VIQ in the left insula (BAs 13, 14, 16) and FSIQ within the inferior frontal gyrus (BAs 44, 45, 47).[92]

Mullen scales of early learning (MSEL) cognitive ability such as visual reception, fine motor, receptive language, expressive language, and early learning composite, has also been found positively correlated with cortical thickness ($r = 0.14$, $p = 0.025$; $r = 0.186$, $p = 0.002$; $r = 0.147$, $p = 0.016$; $r = 0.120$, $p = 0.049$, respectively) of the infants at age 1 year, especially in the bilateral superior frontal and middle frontal gyri (BA 10), right medial superior frontal gyrus (BA 10), right occipital superior gyrus (BA 19), bilateral superior parietal cortices (BA 7), left primary motor cortex (BA 4), bilateral anterior cingulate (BAs 24, 32, 33) and precuneus (BA 4), and right superior and middle temporal cortices (BA 22) areas.[93] Similar findings are also reported for MSEL-based future (at 4 years of age) cognitive score prediction using sMRI brain features at birth such as cortical thickness, mean curvature, local gyrification index, vertex area, vertex volume, sulcal depth in string distance and sulcal depth in Euclidean distance with a mean root square error of 0.067-0.18.[94–96]

Better FSIQ level has also been reported for thinner parietal association cortices, especially left/right inferior parietal (BAs 39, 40) and left/right superior parietal (BA 7) cortices.[97] Overall FSIQ has been found[98–100] correlated ($r = 0.3$~0.7; $p < 0.01$) with the cortical thickness, surface area, sulcal depth, curvature from the left and right parahippocampal gyrus (BA 34), left olfactory cortex (BA 35), right fusiform gyrus (BA 37), bilateral transverse temporal gyri (BAs 41, 42), bilateral thalamus, left parahippocampal gyrus (BA 34), left hippocampus, right opercular part of inferior frontal gyrus (BAs 44, 45, 47), left anterior cingulate gyrus (BAs 24, 32, 33), right amygdala, left lingual gyrus (BA 19), left superior parietal lobule (BA 7), right inferior parietal lobule (BAs 39, 40), left angular gyrus (BA 39), left paracentral lobule, and left caudate nucleus (BAs 1-4).

Voxel- and Surface-based Morphometry to Infer Neurocognition/Intelligence. VBM[101] and SBM[102] allows the correlation of MRI volume or surface metrics at the voxel or surface vertex level. They are extensions of the correlation at the regional or surface area levels.[103] In Table 5 of the supplementary materials, we summarized existing VBM and SBM-based neurocognitive predictive studies.

Table 4. Summary of sMRI studies correlating cortical surface metrices with neurocognition/intelligence. Acronyms- ABCD: Adolescent Brain Cognitive Development, NIH-TCB: NIH toolbox of neurocognitive battery, LASSO: Least Absolute Shrinkage and Selection Operator, SVM: Support Vector Machine, SVR: Support Vector Regression, CNN: Convolutional Neural Network, ROI: Region of Interest, KNN: K-Nearest Neighbors, MSEL: Mullen Scale of Early Learning, PMAT: Penn Progressive Matrices, RIAS: Reynolds Intellectual Assessment Scales, RPM: Raven's Advanced Progressive Matrices Set, GM: Gross Motor, VR: Visual Reception, FM: Fine Motor, RL: Receptive Language, EL: Expressive Language, ELC: Early Learning Composite, CFT: Cluster Forming Threshold, RMSE: Root Mean Square Error, WISC: Wechsler Intelligence Scale for Children, WAIS: Wechsler Adult Intelligence Scale, ABIDE: Autism Brain Imaging Data Exchange, BOLD: Blood-oxygenation Level-dependent, T1-w: T1-weighted MRI, T2-w: T2-weighted MRI, DWI: Diffusion-weighted Imaging. Probable BAs are not specified for either left or right hemisphere.

Study	Year	N	Age (years)	Dataset	MRI type	MRI features	Regions	Probable BAs	IQ/ Neuro. Test	Normal/ Abnormal	Method	Correlation/ Finding
Zhang et al.[96]	2020	23	0-4	UNC Chapel Hill Early Brain Development Study	T1-w, T2-w	Cortical thickness, mean curvature, local gyrification index, vertex area, vertex volume, sulcal depth in string distance, and sulcal depth in Euclidean distance	Parcellation of the cerebral cortex into 70 anatomically meaningful ROIs	Not specified	VR, FM, RL, EL, and ELC (MSEL)	Normal	CNN	RMSE between the predicted and actual VR, FM, RL, and EL scores is 0.067
Li et al.[90]	2020	68	8	Arkansas Children's Nutrition Center	T1-w	Gray matter volume, surface area, and cortical thickness	Orbitofrontal gyrus, transverse temporal gyri, left superior temporal gyrus, and right anterior cingulate gyrus	11, 12, 41, 42, 22, 24, 32, 33	RIAS	Normal	Spearman's correlation test	RIAS scores showed significant correlations (r = [0.38-0.44], p = [0.005-0.046]) with cortical metrices

doi:10.20944/preprints202302.0452.v2

Tadayon et al.[91]	2020	740	21-35	HCP	T1-w	Cortical thickness, cortical surface area, and cortical gyrification	Superior parietal, left supramarginal, left caudal middle frontal, left pars-opercularis, left inferior temporal, right inferior and middle temporal, right medial orbitofrontal, and right rostral middle frontal regions	7, 40, 22, 44, 20, 21, 11, 12, 10	PMAT and NIH-TCB	Normal	Linear regression	Correlation between the local gyrification, and surface area with *gF* and *gC* are 0.29 and 0.22 ($p < 0.001$), 0.28 and 0.28 ($p < 0.001$), respectively
Oxtoby et al.[84]	2019	8669	9-10	ABCD	T1-w	Cortical morphology as graph	A structural co-variance network graph considers small cortical regions (3 voxels cubed) as nodes, and structural similarity (morphology) between nodes as edges.	11, 44, 45, 47, 4, 1, 2, 3, 10, 12, 40	NIH-TCB	Normal	Event-based model of progression, and SVR	Mean Square Error *(gF)* = 93.83 (for true residual *gF* in the range of [-40, 30])
Rebsamen et al.[85]	2019	8669	9-10	ABCD	T1-w	Subcortical volumes, cortical thicknesses, curvatures, and surface areas	Middle temporal gyrus, superior temporal gyrus	21, 22	NIH-TCB	Normal	SVR	Mean Square Error *(gF)* = 93.03 (for true residual *gF* in the range of [-40, 30])
Valverde et al.[86]	2019	8669	9-10	ABCD	T1-w	122 ROI volumes in the gray matter, white matter,	Gray matter, white matter, and cerebrospinal fluid	Not specified	NIH-TCB	Normal	Fully connected neural network	Mean Square Error *(gF)* = 94.02 (for true residual

doi:10.20944/preprints202302.0452.v2

						and cerebrospinal fluid, 78 contrast and 78 cortical thickness measures, gender, age, and scanner manufacturer					*gF* in the range of [-40, 30])
Pölsterl et al.[87]	2019	8669	9-10	ABCD	T1-w	Cortical thickness and volumes of 122 ROIs in the gray matter, white matter, and cerebrospinal fluid	Left/right parahippocampal gyrus, pons white matter, hippocampus, posterior cingulate gyrus, cuneus, left lingual gyrus, left middle frontal gyrus, supramarginal gyrus, right fusiform gyrus, superior temporal gyrus, right anterior cingulate gyrus, etc.	34, 23, 31, 19, 10, 40, 37, 22, 24, 32, 33	NIH-TCB	Normal	An ensemble of gradient boosted trees, and a linear ridge regressor.	Mean Square Error *(gF)* = 94.25 (for true residual *gF* in the range of [-40, 30])
Pölsterl et al.[88]	2019	8669	9-10	ABCD	T1-w	Cortical thickness and volumes of 122 ROIs in the gray matter, white matter, and	Left/right parahippocampal gyrus, pons white matter, hippocampus, posterior cingulate gyrus, cuneus, left lingual gyrus,	34, 23, 31, 19, 10, 40, 37, 22, 24, 32, 33	NIH-TCB	Normal	AutoML ensembles of 14 classifiers	Mean Square Error *(gF)* = 94.25 (for true residual *gF* in the range of [-40, 30])

doi:10.20944/preprints202302.0452.v2

						cerebrospinal fluid	left middle frontal gyrus, supramarginal gyrus, right fusiform gyrus, superior temporal gyrus, right anterior cingulate gyrus, etc.				
Guerdan et al.[89]	2019	8669	9-10	ABCD	T1-w	Volume, elongation, surface area, roundness, and flatness of grey matter ROIs.	Gray matter, white matter, and cerebrospinal fluid	Not specified	NIH-TCB	Normal	LASSO, ridge regressor, SVR, gradient boosting, and AdaBoost regressors.	Mean Square Error *(gF)* = 94.48 (for true residual *gF* in the range of [-40, 30])
Girault et al.[93]	2019	487	1-2	University of North Carolina (UNC) Chapel Hill Early Brain Development Study	T1-w, T2-w	Cortical thickness, and surface area	Bilateral superior frontal and middle frontal gyri, right medial superior frontal gyrus, right occipital superior gyrus, bilateral superior parietal cortices, left primary motor cortex, bilateral anterior cingulate and precuneus, and right superior and middle temporal cortices areas	10, 19, 7, 4, 24, 32, 33. 22	GM, VR, FM, RL, EL, and ELC (MSEL)	Normal	Pearson correlation, Linear mixed effect model	Correlations between average cortical thickness at age 1 and GM, FM, EL, and RL scores at age 1 (r = 0.137, p = 0.025; r = 0.186, p = 0.002; r = 0.147, p = 0.016; r = 0.120, p = 0.049, respectively),

doi:10.20944/preprints202302.0452.v2

Adeli et al.[94]	2019	24	0-4	UNC Chapel Hill Early Brain Development Study	T1-w, T2-w, DWI	Cortical thickness, mean curvature, local gyrification index, vertex area, vertex volume, sulcal depth in string distance, and sulcal depth in Euclidean distance	Parcellation of the cerebral cortex into 70 anatomically meaningful ROIs	Not specified	VR, FM, RL, EL, and ELC (MSEL)	Normal	Multi-task multi-linear regression	RMSE between the predicted and actual VR, FM, RL, and EL scores is 0.18.
Zhang et al.[95]	2018	23	0-4	UNC Chapel Hill Early Brain Development Study	T1-w, T2-w	Cortical thickness, mean curvature, local gyrification index, vertex area, vertex volume, sulcal depth in string distance, and sulcal depth in Euclidean distance	Parcellation of the cerebral cortex into 70 anatomically meaningful ROIs	Not specified	VR, FM, RL, EL, and ELC (MSEL)	Normal	Multi-task multi-linear regression	RMSE between the predicted and actual VR, FM, RL, and EL score is 0.158.
Bajaj et al.[92]	2018	56	18-45	McLean Hospital and Partners Healthcare, and the U.S. Army Human	T1-w	Cortical thickness, cortical surface area, cortical volume, and	Posterior frontal, superior and inferior parietal lobes, left insula, and inferior frontal gyrus	7, 39, 40, 13, 14, 16, 44, 45, 47	WASI-II	Normal	Generalized linear model	Significant positive relationships between thicker cortex and higher IQ at a

doi:10.20944/preprints202302.0452.v2

				Research Protections Office		cortical gyrification					liberal CFT of $p < 0.05$ as well as at a strict CFT of $p < 0.01$ is observed.
Wang et al.[99]	2015	164	6-15	ABIDE	T1-w	Cortical thickness, surface area, sulcal depth, curvature	Bilateral transverse temporal gyri, bilateral thalamus, left parahippocampal gyrus, left hippocampus, right opercular part of inferior frontal gyrus, left anterior cingulate gyrus, right amygdala, left lingual gyrus, left superior parietal lobule, right inferior parietal lobule, left angular gyrus, left paracentral lobule, and left caudate nucleus	41, 42, 34, 44, 45, 47, 32, 7, 40, 39, 1, 2, 3, 4	-	Normal	Multi/single kernel support vector regressor	Correlation between the actual and estimated IQ is 68.4%
Squeglia et al.[97]	2013	185	12-14	San Diego area public middle schools	T1-w	Cortical thickness	Left and right inferior parietal cortices, and left and right superior parietal cortices	39, 40, 7	WISC-III, WAIS-IV	Normal	Hierarchical linear regressions	For both males and females, thinner parietal association cortices corresponded with better neurocognitive functioning

doi:10.20944/preprints202302.0452.v2

											above and beyond age alone.
Yang et al.[98]	2013	78	17-27	Seoul National University, Catholic University of Korea	T1-w	Cortical thickness, surface area, sulcal depth and absolute mean curvature in 78 parcellated ROIs	Cerebral cortex	34, 35, 37	WAIS	Normal	Partial least square regression	Correlation between the Actual and predicted FSIQ is 30% ($p < 0.01$)
Choi et al.[100]	2008	225	20.9±2.9	Seoul National University, Catholic University of Korea	T1-w	The thickness of the gray matter of the cerebral cortex	Gray matter of cerebral cortex	38, 20, 21, 40	WASI, RPM-II	Normal	Multivariate regression model	*gC* is correlated to cortical thickness and *gF* is related to BOLD signals.

Table 5. Summary of sMRI study using brain morphometry in inferring/relating to human neurocognition and intelligence. Acronyms- COPD: Chronic Obstructive Pulmonary Disorder, OCD: Obsessive Compulsive Disorder, DD: Developmental Dyslexia, FA: fractional anisotropy, VBM: Voxels-based Morphometry, MDD: major Depressive Disorder, NCANDA: National Consortium on Alcohol and Neurodevelopment in Adolescence, WASI: Weschler Abbreviated Scale of Intelligence, WISC: Wechsler Intelligence Scale for Children, WAIS: Wechsler Adult Intelligence Scale, FSIQ: Full-scale Intelligent Quotient, VIQ: Verbal IQ, PIQ: Performance IQ, ANCOVA: Analysis of Covariance, T1-w: T1-weighted MRI.

Study	Year	N	Age (years)	Dataset	MRI type	MRI features	Regions	Probable BAs	IQ/ Neuro. Test	Normal/ Abnormal	Method	Correlation/ Finding
Hidese et al.[104]	2020	266	45.6±12.9	Volunteer data from Kodaira city, Tokyo	T1-w, DTI	Regional gray matter volumes in the VBM and the white matter FA	Left gyrus rectus and anterior cingulate gyrus, left posterior insula, left superior and	11, 24, 32, 33, 13, 14, 16, 10	WAIS-III	Normal	Pearson correlation	VIQ correlated positively with the specified brain regional volumes with $p < 0.005$.

doi:10.20944/preprints202302.0452.v2

						values in the DTI	middle frontal gyri				
McDermott et al.[105]	2019	623	5-25	National Institute of Mental Health Intramural Research Program	T1-w	Surface-based shape	Left inferior and middle temporal, left inferior parietal, and left medial frontal regions	20, 21, 39, 40, 25	WASI, WISC, WAIS	Normal	Linear mixed-effect model	Positive associations ($\beta > 100$; $p < 0.001$) between FSIQ and cortical anatomy is observed.
Ramsden et al.[106]	2011	33	14.1±1.0	Department of Psychological Sciences, Birkbeck College, University of London	T1-w	Changes in gray matter density	Motor speech area, and anterior cerebellum	4, 6	WISC, WAIS	Normal	Linear regression	Correlation between change in VIQ and change in grey matter density were 0.876 ($p < 0.01$) for high, 0.797 ($p < 0.05$) for average and 0.660 ($p < 0.05$) for low ability groups, respectively. For PIQ, correlation was 0.492 ($p > 0.05$) for high, 0.788 ($p < 0.05$) for average and 0.715 ($p < 0.01$) for low ability groups, respectively.

doi:10.20944/preprints202302.0452.v2

 doi:10.20944/preprints202302.0452.v2

Briefly, VBM-based gray matter volumes in the left gyrus rectus (BA 11) and anterior cingulate gyrus (BAs 24, 32, 33), left posterior insula (BAs 13, 14, 16), left superior and middle frontal gyri (BA 10) are found to be positively correlated ($p < 0.005$) to VIQ scores.[104] Similarly SBM-base shape features in the left inferior and middle temporal (BAs 20, 21), left inferior parietal (BAs 39, 40), and left medial frontal (BA 25) regions showed positive associations ($\beta > 100$; $p < 0.001$) with FSIQ.[105] Another study[106] divided their study population into average (FSIQ = [80, 119]), low, and high (FSIQ > 119) groups, and observed that the correlation between the change in VIQ and change in the grey matter density in the motor area (BAs 4, 6) and anterior cerebellum is 0.876 ($p < 0.01$) for high ability, 0.797 ($p < 0.05$) for average ability and 0.660 ($p < 0.05$) for low ability groups, respectively. Similarly, the corresponding effects were seen for PIQ as 0.492 ($p > 0.05$) for high ability, 0.788 ($p < 0.05$) for average ability, and 0.715 ($p < 0.01$) for low ability groups.

Deep Features from sMRI to Infer Intelligence/Neurocognition. Regional, surface-area, voxel, and vertex-level features, as described above, are so-called handcrafted or hand-engineered features. They carry neuroanatomic meanings and are easy to interpret. On the other hand, the rise of deep learning extracts tens of thousands or even millions of "deep features" from the whole MRI or image patches. Those deep features are extracted from convolutions of images with filters (3×3×3, 5×5×5, or other sizes). Several studies[60,66,107–110] used a convolutional neural network (CNN), a specific type of image-based deep learning technique, on T1-MRI to predict fluid intelligence in adolescents. They predicted the residual fluid intelligence score of more than 4500 adolescents with an MSE ranging from 92 to 103 (for a range of true residual fluid intelligence score of [-40, 30]), as summarized in Table 6 of the supplementary materials. However, the interpretation of deep features is difficult. A potential solution is to choose brain regions beforehand and those regions to deep learning models. For example, Zou et al.[109] used regions from bilateral transverse temporal gyri (BAs 41, 42), bilateral thalamus, left parahippocampal gyrus (BA 34), left hippocampus, right opercular part of inferior frontal gyrus (BAs 44, 45, 47), left anterior cingulate gyrus (BAs 24, 32, 33), right amygdala, left lingual gyrus (BA 19), left superior parietal lobule (BA 7), right inferior parietal lobule (BAs 39, 40), left angular gyrus (BA 39), left paracentral lobule, and left caudate nucleus (BAs 1-4) in their deep learning model to predict *gF* score. However, the choice of such regions may be subjective, the accuracy of prediction was not significantly different from inputting the whole image, and treating regions separately may miss the opportunity to consider those regions jointly in the convolutions. Interpretation of deep learning models can be also achieved by masking or replacing different regions, adding random noise to images, or calculating the saliency, activating, or attention maps.[111–113] Their use in interpreting deep learning prediction of intelligence or neurocognition is yet to be studied.

Summary of sMRI Inference of Neurocognition and Intelligence. In Figure 4, we show a bar plot representing the proportion of our reviewed sMRI papers that used different Brodmann areas in inferring intelligence and neurocognition. For simplicity, we only used the Brodmann areas without mentioning the hemisphere sides.

Table 6. Summary of sMRI studies inferring/relating to human neurocognition and intelligence. Acronyms- ANCOVA: Analysis of Covariance, ABCD: Adolescent Brain Cognitive Development, NIH-TCB: NIH toolbox of neurocognitive battery, LASSO: Least Absolute Shrinkage and Selection Operator, SVM: Support Vector Machine, SVR: Support Vector Regression, CNN: Convolutional Neural Network, ROI: Region of Interest, KNN: K-Nearest Neighbors, WASI: Weschler Abbreviated Scale of Intelligence, WISC: Wechsler Intelligence Scale for Children, WAIS: Wechsler Adult Intelligence Scale, FSIQ: Full-scale Intelligent Quotient, ABIDE: Autism Brain Imaging Data Exchange, T1-w: T1-weighted MRI, T2-w: T2-weighted MRI, DWI: Diffusion-weighted Imaging, DTI: Diffusion Tensor Imaging, TRUST: T2-relaxation under spin tagging. Probable BAs are not specified for either left or right hemisphere.

Study	Year	N	Age (years)	Dataset	MRI type	MRI features	Regions	Probable BAs	IQ/ Neuro. Test	Normal/ Abnormal	Method	Correlation/ Finding
Chiang et al.[60]	2019	8669	9-10	ABCD	T1-w	Total volume, mean signal intensity, and entropy	Visual, fronto-parietal, somatosensory, motor, default mode network, and cingulo opercular network.	6, 8, 9, 22, 41, 42, 17, 18, 19, 1, 2, 3, 5, 7, 4, 6	NIH-TCB	Normal	CNN, and LASSO	Mean Square Error *(gF)* = 95.38 (for true residual *gF* in the range of [-40, 30])
Ranjbar et al.[66]	2019	8669	9-10	ABCD	T1-w	122 ROI volumes in the gray matter, white matter, and cerebrospinal fluid	Gray matter, white matter, and cerebrospinal fluid	11, 44, 45, 47, 4, 1, 2, 3, 10, 12, 40	NIH-TCB	Normal	CNN and random forest	Mean Square Error *(gF)* = 93.64 (for true residual *gF* in the range of [-40, 30])
Vang et al.[107]	2019	8669	9-10	ABCD	T1-w	CNN-learned features	Gray matter, white matter, and cerebrospinal fluid	Not specified	NIH-TCB	Normal	CNN with gradient boosting machine	Mean Square Error *(gF)* = 96.18 (for true residual *gF* in the range of [-40, 30])
Pominova et al.[108]	2019	8669	9-10	ABCD	T1-w	CNN-learned features	Gray matter	Not specified	NIH-TCB	Normal	VoxCNN	Mean Square Error *(gF)* = 93.838 (for true residual *gF* in the

doi:10.20944/preprints202302.0452.v2

												range of [-40, 30])
Zou et al.[109]	2019	8669	9-10	ABCD	T1-w	CNN-learned features	Bilateral transverse temporal gyri, bilateral thalamus, left parahippocampal gyrus, left hippocampus, right opercular part of inferior frontal gyrus, left anterior cingulate gyrus, right amygdala, left lingual gyrus, left superior parietal lobule, right inferior parietal lobule, left angular gyrus, left paracentral lobule, and left caudate nucleus.	41, 42, 34, 44, 45, 47, 24, 32, 33, 19, 7, 39, 40, 1, 2, 3, 4	NIH-TCB	Normal	3D CNN	Mean Square Error *(gF)* = 92.74 (for true residual *gF* in the range of [-40, 30])
Liu et al.[110]	2019	8669	9-10	ABCD	T1-w	CNN-learned features	Skull-stripped whole brain	Not specified	NIH-TCB	Normal	UNet-like encoder/decoder	Mean Square Error *(gF)* = 102.25 (for true residual *gF* in the range of [-40, 30])

doi:10.20944/preprints202302.0452.v2

Preprints (www.preprints.org) | NOT PEER-REVIEWED | Posted: 3 March 2023 doi:10.20944/preprints202302.0452.v2

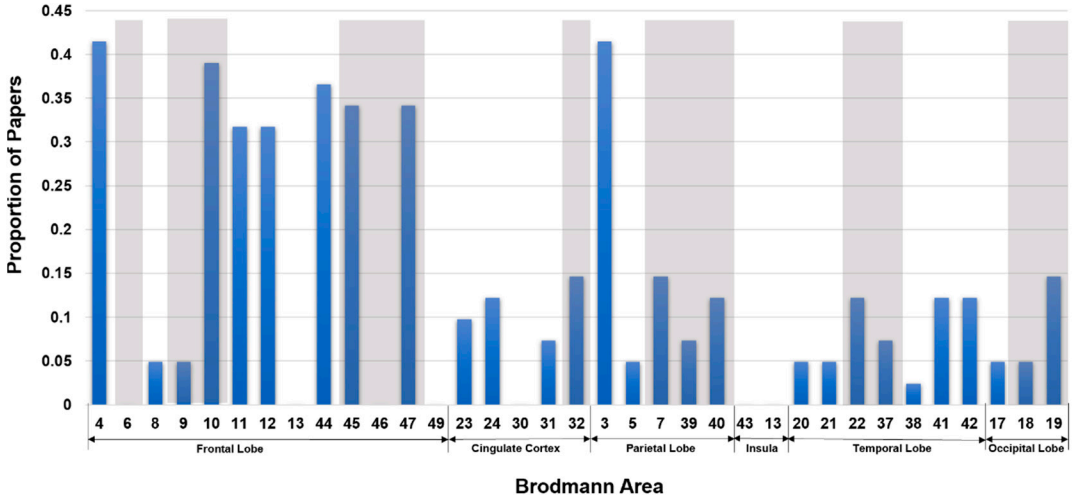

Figure 4. Bar plot representing of the proportion of our reviewed sMRI papers that used different Brodmann areas in inferring intelligence and neurocognition. Shaded BA numbers are part of the P-FIT model. Brodmann areas are not specified for either left or right hemisphere. Studies that did not specify BAs are also included in the normalization.

Diffusion MRI to Infer Intelligence and Neurocognition

Diffusion tensor imaging (DTI) measures water flow at every voxel in the brain. Its parameter maps include Fractional Anisotropy (FA), which measures the directionality of water diffusion (ranging between 0 for complete diffusion in all directions and 1 for single-directional flow), apparent diffusion coefficient (ADC), which measures the magnitude of water diffusion at each voxel. DTI can also construct tractography, which quantifies white matter tracts that water flows through, and is also known as structural connectivity. In Table 7 of the supplementary materials, we summarized existing Diffusion MRI-based neurocognitive predictive studies.

FA is found to be correlated to neurocognitive function. For example, full-scale IQ is shown to be correlated ($r = 0.53$; 95% CI 0.35–0.66) to the FA values in the right anterior thalamic radiation, left superior longitudinal fasciculus, left inferior fronto-occipital fasciculus, and left uncinate fasciculus (collectively, BAs 1, 3-9, 11, 13, 17, 18, 22, 24, 25, 29, 32, 34-36, 38, 39, 41, 42-47).[114] It is also found that FA at 2 weeks of age is correlated ($r = 0.35$-0.48) to the BSID-based neurodevelopmental outcomes at 2 years of age in infants.[115] Similarly, Pearson's correlation analysis revealed a negative correlation ($r = -0.73$; $p < 0.001$) between VIQ and FA in the left-hemispheric Broca's area (BAs 44, 45).[116] In addition, correlation analysis of VIQ and mean diffusivity (MD) revealed a positive correlation in the left hemispheric Broca's area (BAs 44, 45).[116] Another study[117] used FA to find chronic neurological damage in 30-60 years old retired national football league players and its association with mini-mental state examination (MMSE) evaluation of cognitive functions, which revealed a neurophysiological impairment in about 24% of the studied population.

Table 7. Summary of diffusion MRI studies inferring human neurocognition and intelligence. Acronyms- FA: Fractional Anisotropy, MD: Mean Diffusivity, RD: Radial Diffusivity, BSID: Bayley Scales of Infant Development, MSEL: Mullen Scale of Early Learning, MMSE: Mini-Mental Status Examination, VR: Visual Reception, FM: Fine Motor, RL: Receptive Language, EL: Expressive Language, ELC: Early Learning Composite, RMSE: Root Mean Square Error, HCP: Human Connectome Project, WASI: Weschler Abbreviated Scale of Intelligence, WISC: Wechsler Intelligence Scale for Children, WAIS: Wechsler Adult Intelligence Scale, FSIQ: Full-scale Intelligent Quotient, PIQ: Performance IQ, VIQ: Verbal IQ, T1-w: T1-weighted MRI, T2-w: T2-weighted MRI, DWI: Diffusion-weighted Imaging, DTI: Diffusion Tensor Imaging. Probable BAs are not specified for either left or right hemisphere.

Study	Year	N	Age (years)	Dataset	MRI type	MRI features	Regions	Probable BAs	IQ/ Neuro. Test	Normal/ Abnormal	Method	Correlation/ Finding
Malpas et al.[114]	2016	91	18-55	Nathan Kline Institute/Rockland Sample	DTI	FA	42 Brodmann regions were specified in each hemisphere	1, 3, 4, 5, 6, 7, 8, 9, 11, 24, 25, 29, 32, 44, 45, 46, 47, 13, 22, 34, 35, 36, 38, 41, 42, 39, 40, 43, 17, 18	WASI	Normal	*t* statistic regression analysis	FA was positively correlated with FSIQ with r = 0.53 (95% CI 0.35–0.66).
Konrad et al.[116]	2012	30	22.8±1.5	Institute of Neuroradiology of the Johannes Gutenberg University Mainz, Germany	T1-w, DTI	FA, MD	Left-hemispheric Broca's area	44, 45, 22	Hamburg–Wechsler Intelligenztest (HAWIE-R) - equivalent to WAIS-R	Normal	Voxel-wise *t* statistic regression analysis, Pearson correlation	VIQ performance is negatively correlated to the FA in the mentioned regions (r = -0.73; p < 0.001).
Feng et al.[115]	2019	38	0-2	Arkansas Children's Nutrition Center	DTI	FA	White matter tracts	Not specified	BSID-III	Normal	Voxel-wise tract-based spatial statistics (TBSS)	Correlations between FA at 2 weeks of age and BSID subfields scores at 2 years of

doi:10.20944/preprints202302.0452.v2

												age are 0.35~0.48.
Casson et al.[117]	2014	45	30-60	Wayne State University	T1-w, SWI, DTI	FA-based dysarthria, pyramidal system dysfunction, extrapyramidal system dysfunction, and cerebellar dysfunction	Gray matter, white matter, and cerebrospinal fluid	Not specified	MMSE	Normal/ abnormal	Chi-square test	The number of football-related concussions was associated with isolated neurocognitive abnormalities in 24% of population.
Adeli et al.[94]	2019	24	0-4	UNC Chapel Hill Early Brain Development Study	T1-w, T2-w, DWI	Cortical thickness, mean curvature, local gyrification index, vertex area, vertex volume, sulcal depth in string distance, and sulcal depth in Euclidean distance	Parcellation of the cerebral cortex into 70 anatomically meaningful ROIs	Not specified	VR, FM, RL, EL, and ELC (MSEL)	Normal	Multi-task multi-linear regression	Correlation between predicted and true ELC is 0.70 ($p < 0.001$)
Lee et al.[118]	2017	535	0-2	UNC Chapel Hill Early Brain Development Study	DTI	Axial diffusivity (AD), radial diffusivity (RD), and FA	White matter	Not specified	MSEL: ELC	Normal	Distance correlation coefficient	Correlation between AD, RD and FA with ELC are 0.13~0.20 ($p < 0.05$)

doi:10.20944/preprints202302.0452.v2

Zhang et al.[119]	2019	1076	-	HCP	DWI	Count of streamlines, connected surface area (CSA) and weighted CSA, mean and maximum values of FA and MD, cluster number, average length, and mean deviations from a template streamline	ROIs in the whole cortex	Not specified	Raven's Progressive Matrices	Normal	Tensor network principal components analysis	Correlation between actual and estimated *gF* is 24.11% ($p < 0.001$).

doi:10.20944/preprints202302.0452.v2

Preprints (www.preprints.org) | NOT PEER-REVIEWED | Posted: 3 March 2023 doi:10.20944/preprints202302.0452.v2

Other study[94] used different cortical features from the whole brain such as the sulcal depth as Euclidian distance from the cerebral hull surface, local gyrification index, curved sulcal depth along the streamlines constrained in cerebral fluid, mean curvature, and cortical thickness, corresponding to working memory, attention, verbal learning and memory, visuospatial functioning, spatial planning, and problem-solving, and inhibition as features and found a correlation between predicted and true early learning composite (ELC) od 0.70 ($p < 0.001$). A similar study[118] but using DTI-based features from the whole brain such as axial diffusivity (AD), radial diffusivity (RD), and FA found a correlation between the DT features (i.e., AD, RD, and FA) and ELC of 0.13~0.20 ($p < 0.05$). Another study[119] used several DWI features from the whole brain such as count of streamlines, connected surface area (CSA), weighted CSA, mean and maximum FA and MD, cluster number, average length, and mean deviations from a template streamline to predict *gF*, and reported a correlation between actual and estimated *gF* of 24.11% ($p < 0.001$).

Functional MRI to Infer Intelligence and Neurocognition

Functional MRI (fMRI) utilizes the blood oxygenation level-dependent (BOLD) effect to reveal the brain connectivity during a stimulation (task-fMRI) or in a resting state (rs-fMRI).[120] Major large-scale brain networks as found in resting-state fMRI include the dorsal and ventral default mode, right and left executive control, dorsal and ventral attention, anterior and posterior salience, basal ganglia, language, high and primary visual, precuneus, auditory and somatosensory networks, and others.[121]

Functional connectivity strength among different parts of the brain, estimated from fMRI, can be used to predict neurocognitive and intelligence scores. As summarized in Table 8 of the supplementary materials, functional connectivity in the bilateral dorsolateral prefrontal cortices (BA 9) is significantly correlated ($r = 0.47$; $p = 0.0002$) to the Wechsler Adult Intelligence Scale (WAIS) intelligence scores.[122] Also, the functional connectivity in the frontoparietal network region (including BAs 9, 4, 39, 40, 46, 10, 13 and other regions) and central brain regions (i.e., somatosensory region; BAs 1, 2, 3) is used for later life neuropsychological test performance prediction with a correlation between the actual and predicted behavioral scores of $r = 0.12$~0.44 ($p < 0.001$).[123] Frontoparietal network (BAs 9, 4, 39, 40, 46, 10, 13, etc.) connectivity is also found significantly correlated to fluid intelligence ($r = 0.50$; $p < 0.01$),[124] memory ($r = 0.097$; $p < 0.001$),[125] general neurocognitive ability ($r = 0.31$; $p < 0.0001$),[126] and FSIQ ($r = 0.51$; $p < 0.001$)[127] performance. Any disease (e.g. Turner syndrome[128]) related impairment in the fronto-parietal network also causes a deficit in the *gF*/VIQ, compared to a healthy population ($p < 0.0001$).

Some other studies used fMRI-based functional connectivity data from Human Connectome Project (HCP) to show a correlation between the actual and estimated fluid intelligence (0.19-33)[129–133] and cognitive ability (0.95).[134]

In Figure 5, we show a bar plot representing the proportion of our reviewed fMRI papers that used different Brodmann areas in inferring intelligence and neurocognition. For simplicity, here also, we only used the Brodmann areas without mentioning the hemisphere sides. We see in this figure that AI approaches also utilized those Brodmann areas, which were previously reported to be correlated to the intelligence and neurocognition of humans. In addition, we see in this figure that the AI approaches used many Brodmann areas, which are in fact a part of the well-known P-FIT model.

Table 8. Summary of functional MRI inferring human neurocognition and intelligence. Acronyms- OASIS: Open Access Series of Imaging Studies, KSHAP: Korean Social Life, Health, and Aging Project, ABCD: Adolescent Brain Cognitive Development, FC: Functional Connectivity, MMSE: Mini-Mental Status Examination, BOLD: Blood-oxygen-level-dependent, ABCD: Adolescent Brain Cognitive Development, NIH-TCB: NIH toolbox of neurocognitive battery, ANOVA: Analysis of Variance, FSIQ: Full-scale Intelligent Quotient, PIQ: Performance IQ, VIQ: Verbal IQ, LASSO: Least Absolute Shrinkage and Selection Operator, CNN: Convolutional Neural Network, HCP: Human Connectome Project, WAIS: Wechsler Adult Intelligence Scale, WASI: Wechsler Abbreviated Scale of Intelligence, MMSE: Mini-mental State Examination, CPM: Connectome-Based Predictive Modeling; T1-w: T1-weighted MRI, fMRI: functional MRI.

Study	Year	N	Age (years)	Dataset	MRI type	MRI features	Regions	Probable BAs	IQ/ Neuro. Test	Normal/ Abnormal	Method	Correlation/ Finding
Song et al.[122]	2008	59	18.5–33.3	Xuanwu Hospital of Capital Medical University	fMRI	Functional connectivity	bilateral dorsolateral prefrontal cortices	9	WAIS	Normal	Stepwise linear regression	FSIQ is correlated to the functional connectivity in bilateral dorsolateral prefrontal cortices ($r = 0.47$; $p = 0.0002$).
Kwak et al.[123]	2021	795	46-96	OASIS-3, KSHAP	T1-w, fMRI	Functional connectivity from BOLD signals	Region of frontoparietal network and central brain	9, 4, 39, 40, 46, 10, 13, 1, 2, 3	MMSE	Normal	Ridge regression	Correlation between behavioral test scores and FC-predicted score is 0.12~0.44 ($p < 0.001$).
Finn et al.[124]	2015	126	22-35	Human Connectome Project (HCP)	fMRI	Positive and negative edges, frontoparietal networks	Frontoparietal region	9, 4, 39, 40, 46, 10, 13	Raven's Progressive Matrices	Normal	CPM	Correlation between actual and estimated *gF* is 0.5 ($p < 0.01$)
Powell et al.[125]	2017	841	22-37	HCP	fMRI	Voxel-wise local structural connectome	Region of frontoparietal network	9, 4, 39, 40, 46, 10, 13	NIH-TCB	Normal	LASSO Principal Component Regressor	Correlation between the actual and predicted NIH picture sequence

doi:10.20944/preprints202302.0452.v2

											memory test is 0.097 ($p < 0.001$)
Sripada et al.[126]	2020	2013	9-10	ABCD	fMRI	Resting-state functional connectivity pattern	Default mode network, frontoparietal network, salience network, dorsal attention network	8, 9, 10, 21, 28, 36, 23, 24, 32, 29, 30, 31, 39, 40	NIH-TCB	Normal	Brain basis set (BBS) modeling (combination of PCA and linear regression)	General neurocognitive ability score is highly correlated to the mentioned networks ($r = 0.31$; $p < 0.0001$)
Jiang et al.[127]	2017	360	17-24	University of Electronic Science and Technology, China	fMRI	Functional connectivity	Superior frontal gyrus, inferior and superior parietal lobules	10, 11, 12, 39, 40, 7	WAIS-RC	Normal	RelieF+LASSO	Correlation between actual and estimated FSIQ is 51% ($p < 0.001$)
Hart et al.[128]	2006	25	14-29	UNC Pediatric Endocrinology Turner Syndrome Clinic	fMRI	Activated voxels in fMRI	Left and right middle frontal gyri, inferior frontal gyri, intraparietal sulci and inferior temporal gyri	10, 44, 45, 47, 20	WASI	Normal/ abnormal	ANOVA	Individuals with Turner syndrome and controls had significantly different verbal IQs ($p < 0.0001$)
Greene et al.[129]	2018	1086	8-36	HCP, Philadelphia Neurodevelopmental Cohort (PNC)	fMRI	Whole brain functional connectivity	Cortical and subcortical grey matter, cerebellum	Not specified	Raven's Progressive Matrices	Normal	CPM	Correlation between actual and estimated *gF* is 19% in resting state ($p = 0.039$)
He et al.[131]	2018	9821	22-69	HCP, UK-Biobank	fMRI	Functional Connectivity Matrix	Whole-brain spatially independent components	Not specified	Raven's Progressive Matrices	Normal	Kernel Regression, Feedforward NN, CNN	Correlation between actual and estimated *gF* is 23.9% ($p < 0.001$) using the Kernel regression

doi:10.20944/preprints202302.0452.v2

Li et al.[132]	2018	100	-	HCP	fMRI	Amplitude of low-frequency fluctuation of left anterior cingulate cortex	Right prefrontal cortex, left anterior cingulate cortex	8, 24, 32, 33	Raven's Progressive Matrices	Normal	Support vector regressor	Correlation between actual and estimated *gF* is 32.5% ($p = 0.031$)
Dubois et al.[133]	2018	884	22-36	HCP	fMRI	Functional Connectivity Matrix	Cortical and subcortical grey matter	Not specified	Raven's Progressive Matrices	Normal	Univariate correlation filtering + Elastic net regression	Correlation between actual and estimated *gF* is 22% using the univariate model ($p < 0.001$)
Yoo et al.[134]	2019	575	22-56	HCP	fMRI	Functional Connectivity Matrix	Regions of frontoparietal and default mode networks	9, 4, 39, 40, 46, 10, 13, 38, 25, 23, 31	Raven's Progressive Matrices	Normal	CPM-based Multivariate distance correlation	Correlation between actual and estimated cognitive ability is 9.5% ($p < 0.01$)
Noble et al.[135]	2017	618	22-56	HCP	fMRI	10 functionally coherent networks	Whole gray matter	Not specified	Raven's Progressive Matrices	Normal	CPM	Correlation between actual and estimated *gF* is 22% ($p < 0.0001$)

doi:10.20944/preprints202302.0452.v2

Preprints (www.preprints.org) | NOT PEER-REVIEWED | Posted: 3 March 2023 doi:10.20944/preprints202302.0452.v2

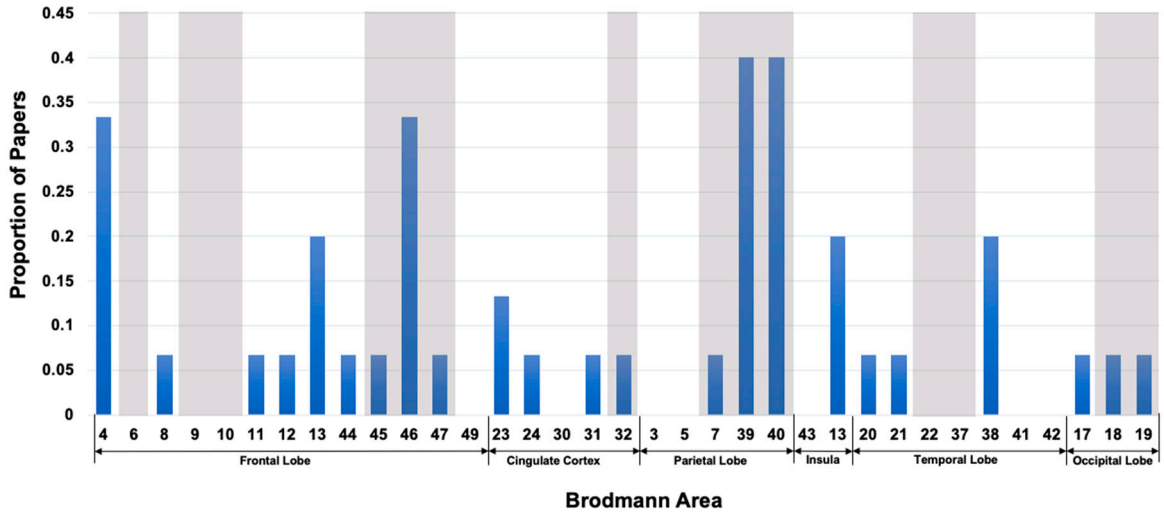

Figure 5. Bar plot representing of the proportion of our reviewed fMRI papers that used different Brodmann areas in inferring intelligence and neurocognition. Shaded BA numbers are part of the P-FIT model. Brodmann areas are not specified for the either left or right hemisphere. Studies that did not specify BAs are also included in the normalization.

Opportunities and Challenges

Precision and Individual Variability. Earlier studies associated MRI metrics with neurocognition in a population. Population-level association does not explain individual variability. There is a need to use MRI to estimate or predict neurocognition for individual subjects. A fundamental question remains open for which MRI metrics, out of hundreds of s/d/fMRI metrics, from which neuroanatomy, carry the neurocognitive information for individual differences. The answers to this question may vary by the neurocognitive domains.

Neuroscientific Interpretation. Sex differences exist widely in diseases[136] and in normal brain MRIs.[137] Hemispheric differences exist and contribute to brain development. Besides sex and hemispheric differences, brain development presents spatial and temporal heterogeneity. Spatially, maturation occurs in a posterior-to-anterior and inferior-to-superior direction[138,139]. Temporally, sensory and motor cortices develop earlier, while the prefrontal, amygdala, and hippocampus continue to get matured during adolescence[139,140], and working memory[141] and reasoning[142] continue to evolve over childhood and adolescence. Yet, it remains open to 'localizing' the regional brain biomarkers in space, in time, and specific to sex, age, and brain hemisphere. Elucidating the neural substrate of inter-individual intelligence difference will also differ across neurocognitive domains.

Nature and nurture beyond MRI data. A mystery is which extent is human intelligence or neurocognition decided by nature (i.e., genetics) and by nurture. For nurture, social upbringing[143] and neighborhood environment[144] have effects on neurodevelopment, so do demographics (age, sex, body mass index or BMI, etc.), lifestyle (smoking, alcohol, reading, exercise, etc.), nutrition, socioeconomic status (education, income, etc.), and other factors. Thus, we need to combine MRI with other nature and nurture data to better understand individual variability in neurocognition.[3,145–150] There are technical challenges for (i) how to best combine 3D MRIs with 1D non-MRI features[151]; (ii) how to identify the best subset of variables that best estimate neurocognitive abilities[152,153]; and (iii) eventually quantify the contribution of nature versus nurture.

Merging Datasets. Artificial intelligence requires a large training dataset, which, for brain MRI, means 1,000 or more subjects.[154] Recent studies have combined public or private datasets to form a large database of thousands or even tens of thousands of brain MRIs, for age prediction,[155,156] quantification of normal brain development,[131] genotype-phenotype mapping[157] and other tasks. We have found at least 38 public datasets with a total of about 35,000 unique individuals with both brain MRIs and neurocognitive/intelligence test scores (Table 2). Challenges arise, however, for (a) multi-site, multi-scanner, multi-protocol MRI harmonization; (b) dealing with different types or versions of

Preprints (www.preprints.org) | NOT PEER-REVIEWED | Posted: 3 March 2023 doi:10.20944/preprints202302.0452.v2

neurocognitive tests as used in different datasets; (c) tackling uncertainties in the test scores for neurocognition/intelligence; and (d) coping with incompleteness or inconsistency in other variables (demographics, socioeconomic status, genetics, environment, etc.) across datasets.

Table 2. We have found at least 38 public datasets with a total of about 35,000 unique individuals with both brain MRIs and neurocognitive/intelligence test scores.

Data Sources			ABCD	ABIDE-I	ABIDE-II	ADNI-1	ADNIGO/2	ADNI-3	AIBL	BeijingEn	BeijingEOEC	BeijingEOEC-II	Berlin	BGSP	CamCAN	CMI	CoRR	DLBS	NIH-PD	NKI-Rockland	Enhan. NKI-RS	HCP-Dev.	HCP-Y.A.	HCP-Aging	Huaxi	IXI-600	MCIC	NIFD	NYU	OASIS-3	PING	PNC	PPMI	QValencia	SALD	SLIM	1000FC	COBRE	NMorphCH	UKBB
N			11,873	567	593	229	188	106	610	180	48	20	50	1,570	653	2,694	1,532	315	548	207	1,335	654	1,206	689	58	595	95	140	49	604	1,493	1,445	74	45	494	580	1,181	74	44	2,201
MRI	Structural MRI		X	X	X	X	X	X	X	X	X	X	X	X	X	X	X	X	X	X	X	X	X	X	X	X	X	X	X	X	X	X	X	X	X	X	X	X	X	X
	Diffusion MRI		X	X	X		X	X		X	X				X	X	X	X	X	X	X	X	X	X	X	X	X		X	X	X	X			X		X	X	X
	Functional MRI		X	X	X		X	X		X	X	X	X	X	X	X	X	X		X	X	X	X	X	X		X		X	X	X		X	X	X	X	X	X	X	X
IQ	General Intelligence			X	X					X				X	X	X	X		X	X	X	X					X		X									X			
	Crystalized Intelligence		X	X	X					X				X	X	X	X	X	X	X	X	X					X	X	X		X							X		X	
	Fluid Intelligence		X	X	X				X	X				X	X	X	X	X	X	X	X	X	X		X		X		X			X				X		X		X	
	Academic Achievement				X											X			X		X						X									X		X			
	Cognition Battery		X	X	X											X			X		X	X	X	X							X	X						X			
	Reaction Time		X	X	X	X	X	X	X						X	X		X	X	X	X	X	X	X			X	X		X	X		X					X		X	
Neurocognition	Language	Expressive Vocabulary				X	X	X	X						X	X		X	X									X		X											
		Receptive Language	X	X	X									X	X	X		X	X			X	X	X				X			X									X	
		Verbal Fluency				X	X	X	X							X		X	X	X	X						X	X		X			X							X	
		Reading	X			X	X		X									X				X	X	X								X						X			
	Memory	Short-term Memory	X	X	X	X			X						X	X		X	X		X	X	X	X			X	X		X	X	X	X							X	
		Episodic Memory	X	X		X	X	X	X							X		X	X		X	X	X	X			X	X		X	X	X	X							X	
		Semantic Memory	X	X		X	X	X	X					X	X	X		X	X			X	X	X			X	X		X	X										X	
	Executive Function	General			X				X										X	X	X						X														
		Attention	X	X					X							X		X	X	X	X	X	X	X			X				X	X							X		X	
		Strategy			X				X						X				X	X	X			X			X														X	
		Cognitive Flexibility	X	X					X							X		X	X	X	X	X	X	X			X				X	X									X	
	Visuospatial		X	X					X						X	X			X	X	X		X	X			X	X					X	X							
	Neurodevelopment				X											X			X																						
	Global Cognition					X	X	X	X						X			X				X	X	X				X		X		X										
	Everyday Functionality					X	X	X								X								X				X		X									X			

Evaluation of the Present versus Prediction of the Future. Predicting future neurocognitive outcomes and intelligence level is more difficult but as, if not more, important than evaluating the current status. Early prediction of later-life neurocognitive outcomes will create a precious time window for early intervention.[7,8] It will identify high-risk patients for targeted intervention, avoiding unnecessary interventions for patients at low risk for future neurocognitive impairments.[158] Both the early and the targeted interventions are key unmet needs in clinical trials that aim to improve patients' long-term neurocognitive outcomes.[8,159] For the last three decades, there have been many studies that used medical imaging (e.g., MRI) and computer-aided mathematical models (e.g., multivariate analysis, machine learning, deep learning, etc.) to identify neurocognitive impairments in patients with various diseases, e.g., traumatic brain injuries,[160] schizophrenia,[161] Alzheimer's Disease,[162] and diabetes.[163] Yet, predicting normal and abnormal neurocognitive development trajectories remains a largely unanswered question.

Linking Healthy and Diseased. Do machine intelligence models that predict human intelligence in normal controls help us to predict abnormal neurocognitive outcomes in diseased populations? Do neurocognitive outcome prediction models share similar MRI and non-MRI features across diseases? Current studies are mostly on diseased populations but studying one specific disease at a

time. Linking healthy and diseased, or merging data across diseases, may offer new insight for the common support of normal and abnormal neurocognitive development.

Conclusion

In this paper, we reviewed different MRI studies to infer neurocognitive or human intelligence. While existing reviews are often on specific disease populations,[164–167] our review focuses primarily on healthy subjects but has included various disease-specific MRI findings. We observed several trends in this research direction: population-level association studies are transitioning to individual-level machine learning predictions, single MRI sequence research is giving ways to multi-modal MRI research, multi-omics approaches integrating MRI with rich non-MRI information are merging from MRI-alone investigations, bigger sample sizes (thousands or tens of thousands) by merging datasets are fast increasing compared to small sample size studies (dozens to hundreds) from a single dataset. Despite growing efforts and expanding knowledge, the decades-long topic of machine intelligence inferring human intelligence remains little understood in general. Opportunities exist with the rise of big data and AI, but several major neuroscientific and data science challenges call for further investigations.

References

1. Morley JE, Morris JC, Berg-Weger M, et al. Brain health: the importance of recognizing cognitive impairment: an IAGG consensus conference. *J Am Med Dir Assoc*. 2015;16(9):731-739.
2. Latal B, Patel P, Liamlahi R, Knirsch W, Tuura RO, von Rhein M. Hippocampal volume reduction is associated with intellectual functions in adolescents with congenital heart disease. *Pediatr Res*. 2016;80(4):531-537.
3. Kessler N, Feldmann M, Schlosser L, et al. Structural brain abnormalities in adults with congenital heart disease: prevalence and association with estimated intelligence quotient. *Int J Cardiol*. 2020;306:61-66.
4. Watson CG, Stopp C, Wypij D, Bellinger DC, Newburger JW, Rivkin MJ. Altered white matter microstructure correlates with IQ and processing speed in children and adolescents post-fontan. *J Pediatr*. 2018;200:140-149. e4.
5. Dubois J, Galdi P, Paul LK, Adolphs R. A distributed brain network predicts general intelligence from resting-state human neuroimaging data. *Philos Trans R Soc B Biol Sci*. 2018;373(1756):20170284.
6. Kanai R, Rees G. The structural basis of inter-individual differences in human behaviour and cognition. *Nat Rev Neurosci*. 2011;12(4):231-242.
7. Liamlahi R, Latal B. Neurodevelopmental outcome of children with congenital heart disease. *Handb Clin Neurol*. 2019;162:329-345.
8. Urschel S, Bond GY, Dinu IA, et al. Neurocognitive outcomes after heart transplantation in early childhood. *J Heart Lung Transplant*. 2018;37(6):740-748.
9. Pallas SL. Intrinsic and extrinsic factors that shape neocortical specification. *Trends Neurosci*. 2001;24(7):417-423.
10. Spitzka EA. Brain-weight, cranial capacity and the form of the head, and their relations to the mental powers of man. *Science*. 1903;17(436):753-754.
11. Pol HEH, Schnack HG, Posthuma D, et al. Genetic contributions to human brain morphology and intelligence. *J Neurosci*. 2006;26(40):10235-10242.
12. Rushton JP, Ankney CD. Whole brain size and general mental ability: a review. *Int J Neurosci*. 2009;119(5):692-732.
13. Deary IJ, Bastin ME, Pattie A, et al. White matter integrity and cognition in childhood and old age. *Neurology*. 2006;66(4):505-512.
14. Schmithorst VJ, Wilke M, Dardzinski BJ, Holland SK. Cognitive functions correlate with white matter architecture in a normal pediatric population: a diffusion tensor MRI study. *Hum Brain Mapp*. 2005;26(2):139-147.
15. Jensen AR. *Clocking the Mind: Mental Chronometry and Individual Differences*. Elsevier; 2006.
16. Poldrack RA, Gorgolewski KJ. Making big data open: data sharing in neuroimaging. *Nat Neurosci*. 2014;17(11):1510-1517.
17. Graham SA, Lee EE, Jeste DV, et al. Artificial intelligence approaches to predicting and detecting cognitive decline in older adults: A conceptual review. *Psychiatry Res*. 2020;284:112732.
18. Dizaji AS, Vieira BH, Khodaei MR, et al. Linking Brain Biology to Intellectual Endowment: A Review on the Associations of Human Intelligence With Neuroimaging Data. *Basic Clin Neurosci*. 2021;12(1):1.
19. Naef N, Schlosser L, Brugger P, et al. Brain volumes in adults with congenital heart disease correlate with executive function abilities. *Brain Imaging Behav*. Published online 2021:1-9.

20. Fontes K, Rohlicek CV, Saint-Martin C, et al. Hippocampal alterations and functional correlates in adolescents and young adults with congenital heart disease. *Hum Brain Mapp*. 2019;40(12):3548-3560.
21. Pike NA, Roy B, Moye S, et al. Reduced hippocampal volumes and memory deficits in adolescents with single ventricle heart disease. *Brain Behav*. 2021;11(2):e01977.
22. Ehrler M, Latal B, Kretschmar O, von Rhein M, Tuura RO. Altered frontal white matter microstructure is associated with working memory impairments in adolescents with congenital heart disease: a diffusion tensor imaging study. *NeuroImage Clin*. 2020;25:102123.
23. McGrew KS. *CHC Theory and the Human Cognitive Abilities Project: Standing on the Shoulders of the Giants of Psychometric Intelligence Research*. Elsevier; 2009.
24. Carroll JB. *Human Cognitive Abilities: A Survey of Factor-Analytic Studies*. Cambridge University Press; 1993.
25. Horn JL, Cattell RB. Refinement and test of the theory of fluid and crystallized general intelligences. *J Educ Psychol*. 1966;57(5):253.
26. Spearmen C. General intelligence objectively determined and measured. *Am J Psychol*. 1904;15:107-197.
27. Cattell RB. Theory of fluid and crystallized intelligence: A critical experiment. *J Educ Psychol*. 1963;54(1):1.
28. Schneider WJ, McGrew KS. The Cattell–Horn–Carroll theory of cognitive abilities. Published online 2018.
29. McGrew K. Cattell-Horn-Carroll CHC (Gf-Gc) Theory: Past, Present & Future.
30. Kaufman AS. *Contemporary Intellectual Assessment: Theories, Tests, and Issues*. Guilford Publications; 2018.
31. Hartman DE. Wechsler Adult Intelligence Scale IV (WAIS IV): return of the gold standard. *Appl Neuropsychol*. 2009;16(1):85-87.
32. Benson N, Hulac DM, Kranzler JH. Independent examination of the Wechsler Adult Intelligence Scale—Fourth Edition (WAIS-IV): what does the WAIS-IV measure? *Psychol Assess*. 2010;22(1):121.
33. Watkins MW, Canivez GL. Assessing the psychometric utility of IQ scores: A tutorial using the Wechsler intelligence scale for children–fifth edition. *Sch Psychol Rev*. Published online 2021:1-15.
34. Wechsler D. *WASI-II: Wechsler Abbreviated Scale of Intelligence*. PsychCorp; 2011.
35. Woodcock RW, McGrew KS, Mather N, Schrank FA. Woodcock-Johnson III diagnostic supplement to the tests of cognitive abilities. *Itasca IL Riverside*. 2003;10:003435520104400407.
36. Bornman J, Romski M, Tonsing K, et al. Adapting and translating the Mullen Scales of Early Learning for the South African context. *S Afr J Commun Disord*. 2018;65(1):1-9.
37. dos Santos ESL, de Kieviet JF, Königs M, van Elburg RM, Oosterlaan J. Predictive value of the Bayley scales of infant development on development of very preterm/very low birth weight children: a meta-analysis. *Early Hum Dev*. 2013;89(7):487-496.
38. Kubinger KD. *Psychologische Diagnostik: Theorie Und Praxis Psychologischen Diagnostizierens*. Hogrefe Verlag; 2006.
39. Wegenschimmel B, Leiss U, Veigl M, et al. Do we still need IQ-scores? Misleading interpretations of neurocognitive outcome in pediatric patients with medulloblastoma: a retrospective study. *J Neurooncol*. 2017;135(2):361-369.
40. Zgaljardic DJ, Temple RO. Neuropsychological Assessment Battery (NAB): Performance in a sample of patients with moderate-to-severe traumatic brain injury. *Appl Neuropsychol*. 2010;17(4):283-288.
41. Akshoomoff N, Beaumont JL, Bauer PJ, et al. VIII. NIH Toolbox Cognition Battery (CB): composite scores of crystallized, fluid, and overall cognition. *Monogr Soc Res Child Dev*. 2013;78(4):119-132.
42. Denboer JW, Nicholls C, Corte C, Chestnut K. *National Institutes of Health Toolbox Cognition Battery*. Oxford University Press; 2014.
43. Barbey AK. Network neuroscience theory of human intelligence. *Trends Cogn Sci*. 2018;22(1):8-20.
44. Duncan J, Owen AM. Common regions of the human frontal lobe recruited by diverse cognitive demands. *Trends Neurosci*. 2000;23(10):475-483.
45. Duncan J. The multiple-demand (MD) system of the primate brain: mental programs for intelligent behaviour. *Trends Cogn Sci*. 2010;14(4):172-179.
46. Kovacs K, Conway AR. Process overlap theory: A unified account of the general factor of intelligence. *Psychol Inq*. 2016;27(3):151-177.
47. Jung RE, Haier RJ. The Parieto-Frontal Integration Theory (P-FIT) of intelligence: converging neuroimaging evidence. *Behav Brain Sci*. 2007;30(2):135-154.
48. Deary IJ, Penke L, Johnson W. The neuroscience of human intelligence differences. *Nat Rev Neurosci*. 2010;11(3):201-211.
49. Colom R, Karama S, Jung RE, Haier RJ. Human intelligence and brain networks. *Dialogues Clin Neurosci*. Published online 2022.
50. Lerch JP, Van Der Kouwe AJ, Raznahan A, et al. Studying neuroanatomy using MRI. *Nat Neurosci*. 2017;20(3):314-326.
51. Fischl B. FreeSurfer. *Neuroimage*. 2012;62(2):774-781.
52. Jenkinson M, Beckmann CF, Behrens TE, Woolrich MW, Smith SM. Fsl. *Neuroimage*. 2012;62(2):782-790.
53. Cox RW. AFNI: what a long strange trip it's been. *Neuroimage*. 2012;62(2):743-747.

54. Eickhoff SB, Yeo BT, Genon S. Imaging-based parcellations of the human brain. *Nat Rev Neurosci*. 2018;19(11):672-686.
55. Zhang-James Y, Glatt SJ, Faraone SV. Nu Support Vector Machine in Prediction of Fluid Intelligence Using MRI Data. In: *Challenge in Adolescent Brain Cognitive Development Neurocognitive Prediction*. Springer; 2019:92-98.
56. Chen H, Dou Q, Yu L, Qin J, Heng PA. VoxResNet: Deep voxelwise residual networks for brain segmentation from 3D MR images. *NeuroImage*. 2018;170:446-455.
57. Tsukahara JS, Harrison TL, Draheim C, Martin JD, Engle RW. Attention control: The missing link between sensory discrimination and intelligence. *Atten Percept Psychophys*. 2020;82(7):3445-3478.
58. Cabeza R, Nyberg L. Imaging cognition II: An empirical review of 275 PET and fMRI studies. *J Cogn Neurosci*. 2000;12(1):1-47.
59. MacDonald AW, Cohen JD, Stenger VA, Carter CS. Dissociating the role of the dorsolateral prefrontal and anterior cingulate cortex in cognitive control. *Science*. 2000;288(5472):1835-1838.
60. Chiang JN, Reggente N, Dell'Italia J, Zheng ZS, Lutkenhoff ES. Predicting Fluid Intelligence Using Anatomical Measures Within Functionally Defined Brain Networks. In: *Challenge in Adolescent Brain Cognitive Development Neurocognitive Prediction*. Springer; 2019:143-149.
61. Srivastava S, Eitel F, Ritter K. Predicting fluid intelligence in adolescent brain mri data: An ensemble approach. In: *Challenge in Adolescent Brain Cognitive Development Neurocognitive Prediction*. Springer; 2019:74-82.
62. Ren H, Wang X, Wang S, Zhang Z. Predict Fluid Intelligence of Adolescent Using Ensemble Learning. In: *Challenge in Adolescent Brain Cognitive Development Neurocognitive Prediction*. Springer; 2019:66-73.
63. Tamez-Pena J, Orozco J, Sosa P, Valdes A, Nezhadmoghadam F. Ensemble of svm, random-forest and the bswims method to predict and describe structural associations with fluid intelligence scores from t1-weighed mri. In: *Challenge in Adolescent Brain Cognitive Development Neurocognitive Prediction*. Springer; 2019:47-56.
64. Brueggeman L, Koomar T, Huang Y, et al. Ensemble Modeling of Neurocognitive Performance Using MRI-Derived Brain Structure Volumes. In: *Challenge in Adolescent Brain Cognitive Development Neurocognitive Prediction*. Springer; 2019:124-132.
65. Mihalik A, Brudfors M, Robu M, et al. ABCD Neurocognitive Prediction Challenge 2019: predicting individual fluid intelligence scores from structural MRI using probabilistic segmentation and kernel ridge regression. In: *Challenge in Adolescent Brain Cognitive Development Neurocognitive Prediction*. Springer; 2019:133-142.
66. Ranjbar S, Singleton KW, Curtin L, et al. Sex differences in predicting fluid intelligence of adolescent brain from T1-weighted MRIs. In: *Challenge in Adolescent Brain Cognitive Development Neurocognitive Prediction*. Springer; 2019:150-157.
67. Wlaszczyk A, Kaminska A, Pietraszek A, Dabrowski J, Pawlak MA, Nowicka H. Predicting Fluid Intelligence from Structural MRI Using Random Forest regression. In: *Challenge in Adolescent Brain Cognitive Development Neurocognitive Prediction*. Springer; 2019:83-91.
68. Kao PY, Zhang A, Goebel M, Chen JW, Manjunath BS. Predicting Fluid Intelligence of Children using T1-weighted MR Images and a StackNet. In: *Challenge in Adolescent Brain Cognitive Development Neurocognitive Prediction*. Springer; 2019:9-16.
69. Li T, Wang X, Luo T, et al. Adolescent Fluid Intelligence Prediction from Regional Brain Volumes and Cortical Curvatures Using BlockPC-XGBoost. In: *Challenge in Adolescent Brain Cognitive Development Neurocognitive Prediction*. Springer; 2019:167-175.
70. Saha S, Pagnozzi A, Bradford D, Fripp J. Predicting fluid intelligence in adolescence from structural MRI with deep learning methods. *Intelligence*. 2021;88:101568.
71. Kane MJ, Engle RW. The role of prefrontal cortex in working-memory capacity, executive attention, and general fluid intelligence: An individual-differences perspective. *Psychon Bull Rev*. 2002;9(4):637-671.
72. Conway AR, Cowan N, Bunting MF, Therriault DJ, Minkoff SR. A latent variable analysis of working memory capacity, short-term memory capacity, processing speed, and general fluid intelligence. *Intelligence*. 2002;30(2):163-183.
73. Paul EJ, Larsen RJ, Nikolaidis A, et al. Dissociable brain biomarkers of fluid intelligence. *Neuroimage*. 2016;137:201-211.
74. Morsing E, Malova M, Kahn A, et al. Brain Volumes and Developmental Outcome in Childhood Following Fetal Growth Restriction Leading to Very Preterm Birth. *Front Physiol*. 2018;9:1583. doi:10.3389/fphys.2018.01583
75. Ogawa T, Aihara T, Shimokawa T, Yamashita O. Large-scale brain network associated with creative insight: combined voxel-based morphometry and resting-state functional connectivity analyses. *Sci Rep*. 2018;8(1):1-11.
76. Hilger K, Winter NR, Leenings R, et al. Predicting intelligence from brain gray matter volume. *Brain Struct Funct*. 2020;225(7):2111-2129.

77. Packard MG, Knowlton BJ. Learning and memory functions of the basal ganglia. *Annu Rev Neurosci*. 2002;25(1):563-593.
78. Tricomi E, Delgado MR, McCandliss BD, McClelland JL, Fiez JA. Performance feedback drives caudate activation in a phonological learning task. *J Cogn Neurosci*. 2006;18(6):1029-1043.
79. Grazioplene RG, G. Ryman S, Gray JR, Rustichini A, Jung RE, DeYoung CG. Subcortical intelligence: Caudate volume predicts IQ in healthy adults. *Hum Brain Mapp*. 2015;36(4):1407-1416.
80. Westlye LT, Walhovd KB, Bjørnerud A, Due-Tønnessen P, Fjell AM. Error-related negativity is mediated by fractional anisotropy in the posterior cingulate gyrus—a study combining diffusion tensor imaging and electrophysiology in healthy adults. *Cereb Cortex*. 2009;19(2):293-304.
81. Bar M, Tootell RB, Schacter DL, et al. Cortical mechanisms specific to explicit visual object recognition. *Neuron*. 2001;29(2):529-535.
82. McCandliss BD, Cohen L, Dehaene S. The visual word form area: expertise for reading in the fusiform gyrus. *Trends Cogn Sci*. 2003;7(7):293-299.
83. McClelland JL, Rogers TT. The parallel distributed processing approach to semantic cognition. *Nat Rev Neurosci*. 2003;4(4):310-322.
84. Oxtoby NP, Ferreira FS, Mihalik A, et al. ABCD Neurocognitive Prediction Challenge 2019: Predicting individual residual fluid intelligence scores from cortical grey matter morphology. In: *Challenge in Adolescent Brain Cognitive Development Neurocognitive Prediction*. Springer; 2019:114-123.
85. Rebsamen M, Rummel C, Mürner-Lavanchy I, Reyes M, Wiest R, McKinley R. Surface-Based Brain Morphometry for the Prediction of Fluid Intelligence in the Neurocognitive Prediction Challenge 2019. In: *Challenge in Adolescent Brain Cognitive Development Neurocognitive Prediction*. Springer; 2019:26-34.
86. Valverde JM, Imani V, Lewis JD, Tohka J. Predicting intelligence based on cortical WM/GM contrast, cortical thickness and volumetry. In: *Challenge in Adolescent Brain Cognitive Development Neurocognitive Prediction*. Springer; 2019:57-65.
87. Pölsterl S, Gutiérrez-Becker B, Sarasua I, Roy AG, Wachinger C. Prediction of Fluid Intelligence from T1-Weighted Magnetic Resonance Images. In: *Challenge in Adolescent Brain Cognitive Development Neurocognitive Prediction*. Springer; 2019:35-46.
88. Pölsterl S, Gutiérrez-Becker B, Sarasua I, Roy AG, Wachinger C. An AutoML Approach for the Prediction of Fluid Intelligence from MRI-Derived Features. In: *Challenge in Adolescent Brain Cognitive Development Neurocognitive Prediction*. Springer; 2019:99-107.
89. Guerdan L, Sun P, Rowland C, et al. Deep learning vs. classical machine learning: A comparison of methods for fluid intelligence prediction. In: *Challenge in Adolescent Brain Cognitive Development Neurocognitive Prediction*. Springer; 2019:17-25.
90. Li T, McCorkle GS, Williams DK, Badger TM, Ou X. Cortical Morphometry is Associated with Neuropsychological Function in Healthy 8-Year-Old Children. *J Neuroimaging*. 2020;30(6):833-842.
91. Tadayon E, Pascual-Leone A, Santarnecchi E. Differential contribution of cortical thickness, surface area, and gyrification to fluid and crystallized intelligence. *Cereb Cortex*. 2020;30(1):215-225.
92. Bajaj S, Raikes A, Smith R, et al. The relationship between general intelligence and cortical structure in healthy individuals. *Neuroscience*. 2018;388:36-44.
93. Girault JB, Cornea E, Goldman BD, et al. Cortical structure and cognition in infants and toddlers. *Cereb Cortex*. 2020;30(2):786-800.
94. Adeli E, Meng Y, Li G, Lin W, Shen D. Multi-task prediction of infant cognitive scores from longitudinal incomplete neuroimaging data. *NeuroImage*. 2019;185:783-792.
95. Zhang C, Adeli E, Wu Z, Li G, Lin W, Shen D. Infant brain development prediction with latent partial multi-view representation learning. *IEEE Trans Med Imaging*. 2018;38(4):909-918.
96. Zhang X, Cheng J, Ni H, et al. Infant Cognitive Scores Prediction with Multi-stream Attention-Based Temporal Path Signature Features. In: *International Conference on Medical Image Computing and Computer-Assisted Intervention*. Springer; 2020:134-144.
97. Squeglia LM, Jacobus J, Sorg SF, Jernigan TL, Tapert SF. Early adolescent cortical thinning is related to better neuropsychological performance. *J Int Neuropsychol Soc*. 2013;19(9):962-970.
98. Yang JJ, Yoon U, Yun HJ, et al. Prediction for human intelligence using morphometric characteristics of cortical surface: partial least square analysis. *Neuroscience*. 2013;246:351-361.
99. Wang L, Wee CY, Suk HI, Tang X, Shen D. MRI-based intelligence quotient (IQ) estimation with sparse learning. *PloS One*. 2015;10(3):e0117295.
100. Choi YY, Shamosh NA, Cho SH, et al. Multiple bases of human intelligence revealed by cortical thickness and neural activation. *J Neurosci*. 2008;28(41):10323-10329.
101. Wright IC, McGuire PK, Poline JB, et al. A voxel-based method for the statistical analysis of gray and white matter density applied to schizophrenia. *Neuroimage*. 1995;2(4):244-252.
102. Kim H, Kim J hoon, Possin KL, et al. Surface-based morphometry reveals caudate subnuclear structural damage in patients with premotor Huntington disease. *Brain Imaging Behav*. 2017;11(5):1365-1372.

103. Whitwell JL. Voxel-based morphometry: an automated technique for assessing structural changes in the brain. *J Neurosci*. 2009;29(31):9661-9664.
104. Hidese S, Ota M, Matsuo J, et al. Correlation Between the Wechsler Adult Intelligence Scale-3 (rd) Edition Metrics and Brain Structure in Healthy Individuals: A Whole-Brain Magnetic Resonance Imaging Study. *Front Hum Neurosci*. 2020;14.
105. McDermott CL, Seidlitz J, Nadig A, et al. Longitudinally mapping childhood socioeconomic status associations with cortical and subcortical morphology. *J Neurosci*. 2019;39(8):1365-1373.
106. Ramsden S, Richardson FM, Josse G, et al. Verbal and non-verbal intelligence changes in the teenage brain. *Nature*. 2011;479(7371):113-116.
107. Vang YS, Cao Y, Xie X. A Combined Deep Learning-Gradient Boosting Machine Framework for Fluid Intelligence Prediction. In: *Challenge in Adolescent Brain Cognitive Development Neurocognitive Prediction*. Springer; 2019:1-8.
108. Pominova M, Kuzina A, Kondrateva E, et al. Ensemble of 3D CNN regressors with data fusion for fluid intelligence prediction. In: *Challenge in Adolescent Brain Cognitive Development Neurocognitive Prediction*. Springer; 2019:158-166.
109. Zou Y, Jang I, Reese TG, Yao J, Zhu W, Rispoli JV. Cortical and Subcortical Contributions to Predicting Intelligence Using 3D ConvNets. In: *Challenge in Adolescent Brain Cognitive Development Neurocognitive Prediction*. Springer; 2019:176-185.
110. Liu L, Yu L, Wang S, Heng PA. Predicting Fluid Intelligence from MRI Images with Encoder-Decoder Regularization. In: *Challenge in Adolescent Brain Cognitive Development Neurocognitive Prediction*. Springer; 2019:108-113.
111. Arrieta AB, Díaz-Rodríguez N, Del Ser J, et al. Explainable Artificial Intelligence (XAI): Concepts, taxonomies, opportunities and challenges toward responsible AI. *Inf Fusion*. 2020;58:82-115.
112. Gunning D, Stefik M, Choi J, Miller T, Stumpf S, Yang GZ. XAI—Explainable artificial intelligence. *Sci Robot*. 2019;4(37):eaay7120.
113. Speith T. A review of taxonomies of explainable artificial intelligence (XAI) methods. In: *2022 ACM Conference on Fairness, Accountability, and Transparency*. ; 2022:2239-2250.
114. Malpas CB, Genc S, Saling MM, Velakoulis D, Desmond PM, O'Brien TJ. MRI correlates of general intelligence in neurotypical adults. *J Clin Neurosci*. 2016;24:128-134.
115. Feng K, Rowell AC, Andres A, et al. Diffusion tensor MRI of white matter of healthy full-term newborns: relationship to neurodevelopmental outcomes. *Radiology*. 2019;292(1):179-187.
116. Konrad A, Vucurevic G, Musso F, Winterer G. VBM–DTI correlates of verbal intelligence: a potential link to Broca's Area. *J Cogn Neurosci*. 2012;24(4):888-895.
117. Casson IR, Viano DC, Haacke EM, Kou Z, LeStrange DG. Is there chronic brain damage in retired NFL players? Neuroradiology, neuropsychology, and neurology examinations of 45 retired players. *Sports Health*. 2014;6(5):384-395.
118. Lee SJ, Steiner RJ, Yu Y, et al. Common and heritable components of white matter microstructure predict cognitive function at 1 and 2 y. *Proc Natl Acad Sci*. 2017;114(1):148-153.
119. Zhang Z, Allen GI, Zhu H, Dunson D. Tensor network factorizations: Relationships between brain structural connectomes and traits. *Neuroimage*. 2019;197:330-343.
120. Gore JC, Li M, Gao Y, et al. Functional MRI and resting state connectivity in white matter-a mini-review. *Magn Reson Imaging*. 2019;63:1-11.
121. Shirer WR, Ryali S, Rykhlevskaia E, Menon V, Greicius MD. Decoding subject-driven cognitive states with whole-brain connectivity patterns. *Cereb Cortex*. 2012;22(1):158-165.
122. Song M, Zhou Y, Li J, et al. Brain spontaneous functional connectivity and intelligence. *Neuroimage*. 2008;41(3):1168-1176.
123. Kwak S, Kim H, Kim H, Youm Y, Chey J. Distributed functional connectivity predicts neuropsychological test performance among older adults. *Hum Brain Mapp*. Published online 2021.
124. Finn ES, Shen X, Scheinost D, et al. Functional connectome fingerprinting: identifying individuals using patterns of brain connectivity. *Nat Neurosci*. 2015;18(11):1664-1671.
125. Powell MA, Garcia JO, Yeh FC, Vettel JM, Verstynen T. Local connectome phenotypes predict social, health, and cognitive factors. *Netw Neurosci*. 2018;2(1):86-105.
126. Sripada C, Rutherford S, Angstadt M, et al. Prediction of neurocognition in youth from resting state fMRI. *Mol Psychiatry*. 2020;25(12):3413-3421.
127. Jiang R, Qi S, Du Y, et al. Predicting individualized intelligence quotient scores using brainnetome-atlas based functional connectivity. In: *2017 IEEE 27th International Workshop on Machine Learning for Signal Processing (MLSP)*. IEEE; 2017:1-6.
128. Hart SJ, Davenport ML, Hooper SR, Belger A. Visuospatial executive function in Turner syndrome: functional MRI and neurocognitive findings. *Brain*. 2006;129(5):1125-1136.
129. Greene AS, Gao S, Scheinost D, Constable RT. Task-induced brain state manipulation improves prediction of individual traits. *Nat Commun*. 2018;9(1):1-13.

130. Elliott ML, Knodt AR, Cooke M, et al. General functional connectivity: Shared features of resting-state and task fMRI drive reliable and heritable individual differences in functional brain networks. *Neuroimage*. 2019;189:516-532.
131. He T, Kong R, Holmes A, et al. Do deep neural networks outperform kernel regression for functional connectivity prediction of behavior. *BioRxiv*. Published online 2018:473603.
132. Li C, Yang G, Li M, Li B. Fluid intelligence relates to the resting state amplitude of low-frequency fluctuation and functional connectivity: a multivariate pattern analysis. *NeuroReport*. 2018;29(1):8-12.
133. Dubois J, Galdi P, Han Y, Paul LK, Adolphs R. Resting-state functional brain connectivity best predicts the personality dimension of openness to experience. *Personal Neurosci*. 2018;1.
134. Yoo K, Rosenberg MD, Noble S, Scheinost D, Constable RT, Chun MM. Multivariate approaches improve the reliability and validity of functional connectivity and prediction of individual behaviors. *Neuroimage*. 2019;197:212-223.
135. Noble S, Spann MN, Tokoglu F, Shen X, Constable RT, Scheinost D. Influences on the test–retest reliability of functional connectivity MRI and its relationship with behavioral utility. *Cereb Cortex*. 2017;27(11):5415-5429.
136. Kanaya AM, Grady D, Barrett-Connor E. Explaining the sex difference in coronary heart disease mortality among patients with type 2 diabetes mellitus: a meta-analysis. *Arch Intern Med*. 2002;162(15):1737-1745.
137. Cosgrove KP, Mazure CM, Staley JK. Evolving knowledge of sex differences in brain structure, function, and chemistry. *Biol Psychiatry*. 2007;62(8):847-855.
138. Sowell ER, Thompson PM, Leonard CM, Welcome SE, Kan E, Toga AW. Longitudinal mapping of cortical thickness and brain growth in normal children. *J Neurosci*. 2004;24(38):8223-8231.
139. Giedd JN, Blumenthal J, Jeffries NO, et al. Brain development during childhood and adolescence: a longitudinal MRI study. *Nat Neurosci*. 1999;2(10):861-863.
140. Herting MM, Johnson C, Mills KL, et al. Development of subcortical volumes across adolescence in males and females: A multisample study of longitudinal changes. *NeuroImage*. 2018;172:194-205.
141. Nagel BJ, Herting MM, Maxwell EC, Bruno R, Fair D. Hemispheric lateralization of verbal and spatial working memory during adolescence. *Brain Cogn*. 2013;82(1):58-68.
142. Vendetti MS, Johnson EL, Lemos CJ, Bunge SA. Hemispheric differences in relational reasoning: novel insights based on an old technique. *Front Hum Neurosci*. 2015;9:55.
143. Steffener J, Habeck C, O'Shea D, Razlighi Q, Bherer L, Stern Y. Differences between chronological and brain age are related to education and self-reported physical activity. *Neurobiol Aging*. 2016;40:138-144.
144. Hackman DA, Cserbik D, Chen JC, et al. Association of Local Variation in Neighborhood Disadvantage in Metropolitan Areas With Youth Neurocognition and Brain Structure. *JAMA Pediatr*. Published online 2021:e210426-e210426.
145. Skotting MB, Eskildsen SF, Ovesen AS, et al. Infants with congenital heart defects have reduced brain volumes. *Sci Rep*. 2021;11(1):1-8.
146. Bolduc ME, Lambert H, Ganeshamoorthy S, Brossard-Racine M. Structural brain abnormalities in adolescents and young adults with congenital heart defect: a systematic review. *Dev Med Child Neurol*. 2018;60(12):1209-1224.
147. Asschenfeldt B, Evald L, Heiberg J, et al. Neuropsychological status and structural brain imaging in adults with simple congenital heart defects closed in childhood. *J Am Heart Assoc*. 2020;9(11):e015843.
148. Oster ME, Watkins S, Hill KD, Knight JH, Meyer RE. Academic outcomes in children with congenital heart defects: a population-based cohort study. *Circ Cardiovasc Qual Outcomes*. 2017;10(2):e003074.
149. Savory K, Manivannan S, Zaben M, Uzun O, Syed YA. Impact of copy number variation on human neurocognitive deficits and congenital heart defects: a systematic review. *Neurosci Biobehav Rev*. 2020;108:83-93.
150. Derridj N, Guedj R, Calderon J, et al. Long-term Neurodevelopmental Outcomes of Children with Congenital Heart Defects. *J Pediatr*. Published online 2021.
151. Huang SC, Pareek A, Seyyedi S, Banerjee I, Lungren MP. Fusion of medical imaging and electronic health records using deep learning: a systematic review and implementation guidelines. *NPJ Digit Med*. 2020;3(1):1-9.
152. Guyon I, Elisseeff A. An introduction to variable and feature selection. *J Mach Learn Res*. 2003;3(Mar):1157-1182.
153. Li J, Cheng K, Wang S, et al. Feature selection: A data perspective. *ACM Comput Surv CSUR*. 2017;50(6):1-45.
154. Smith SM, Nichols TE. Statistical challenges in "big data" human neuroimaging. *Neuron*. 2018;97(2):263-268.
155. He S, Pereira D, Perez JD, et al. Multi-channel attention-fusion neural network for brain age estimation: Accuracy, generality, and interpretation with 16,705 healthy MRIs across lifespan. *Med Image Anal*. 2021;72:102091.

156. He S, Grant PE, Ou Y. Global-Local Transformer for Brain Age Estimation. *IEEE Trans Med Imaging*. Published online 2021.
157. Brookes AJ, Robinson PN. Human genotype–phenotype databases: aims, challenges and opportunities. *Nat Rev Genet*. 2015;16(12):702-715.
158. Sterling LH, Liu A, Ganni E, et al. Neurocognitive disorders amongst patients with congenital heart disease undergoing procedures in childhood. *Int J Cardiol*. Published online 2021.
159. Calderon J, Bellinger DC. Executive function deficits in congenital heart disease: why is intervention important? *Cardiol Young*. 2015;25(7):1238-1246.
160. Cole JH, Leech R, Sharp DJ, Initiative ADN. Prediction of brain age suggests accelerated atrophy after traumatic brain injury. *Ann Neurol*. 2015;77(4):571-581.
161. Cole JH, Ritchie SJ, Bastin ME, et al. Brain age predicts mortality. *Mol Psychiatry*. 2018;23(5):1385.
162. Franke K, Ziegler G, Klöppel S, Gaser C, Initiative ADN. Estimating the age of healthy subjects from T1-weighted MRI scans using kernel methods: exploring the influence of various parameters. *Neuroimage*. 2010;50(3):883-892.
163. Franke K, Gaser C, Manor B, Novak V. Advanced BrainAGE in older adults with type 2 diabetes mellitus. *Front Aging Neurosci*. 2013;5:90.
164. Antonova E, Sharma T, Morris R, Kumari V. The relationship between brain structure and neurocognition in schizophrenia: a selective review. *Schizophr Res*. 2004;70(2-3):117-145.
165. Berkelhammer LD, Williamson AL, Sanford SD, et al. Neurocognitive sequelae of pediatric sickle cell disease: a review of the literature. *Child Neuropsychol*. 2007;13(2):120-131.
166. Shields LB, Choucair AK. Management of low-grade gliomas: a review of patient-perceived quality of life and neurocognitive outcome. *World Neurosurg*. 2014;82(1-2):e299-e309.
167. Subramaniyan S, Terrando N. Narrative review article: neuroinflammation and perioperative neurocognitive disorders. *Anesth Analg*. 2019;128(4):781.